THE TEMPORAL EVOLUTION OF TORNADIC AND NON-TORNADIC VORTEX2 NEAR-STORM ENVIRONMENTS

by

Austin Daniel Mansfield

A thesis submitted to the faculty of
The University of North Carolina at Charlotte
in partial fulfillment of the requirements
for the degree of Master of Science in
Earth Sciences

Charlotte

2019

Approved by:

_____
Dr. Casey Davenport

_____
Dr. Matthew Eastin

_____
Mr. Terry Shirley

ABSTRACT

AUSTIN DANIEL MANSFIELD. The Temporal Evolution of Tornadic and Non-Tornadic VORTEX2 Near-Storm Environments. (Under the direction of DR. CASEY DAVENPORT)

The VORTEX2 field experiment provided a wealth of data on the near-storm environments of tornadic and non-tornadic supercell thunderstorms. While previous research has documented the spatial heterogeneity associated with the environment in the vicinity of the VORTEX2 storms, this study focuses on the temporal evolution of the near-storm environment. Thirty-seven supercells are examined (11 tornadic, and 26 non-tornadic), each with at least three near inflow soundings launched throughout the lifetime of the supercell. The evolution of common forecasting parameters (including shear, storm-relative helicity and instability) are compared among the tornadic and non-tornadic categories. Each parameter is analyzed individually as well as grouped with similar measures to understand potential connections with storm behavior on a temporal track. The timing of associated storms is examined to identify relationships between environmental trends and observed hazards. Each parameter is quantified based off of a time series average along with the average time of tornadogenesis (22:26 UTC). The distribution of each parameter values between tornadic and non-tornadic cases are also illustrated using a violin plot. Parameter values are also examined relative to times of tornadogenesis, peak mesocyclone intensity (for non-tornadic cases), and sunset. After initial observations are made, a statistical analysis was conducted to quantitatively see if there were any statistical differences between the tornadic and non-tornadic cases in regards to the entire dataset (1st thru 3rd soundings). Thus, creating a new comprehension

of finding discriminatory parameters (if any) relative to tornadogenesis thus benefiting future tornado forecasting methodologies.

ACKNOWLEDGEMENTS

Thank you to my advisor, Dr. Casey Davenport for being exactly the kind of motivation I needed as a graduate student coming from East Carolina. I needed a go-getter of an advisor to keep me on my toes and always working and I thank you for living up to those ideas. Thank you to my committee members, Mr. Terry Shirley and Dr. Matthew Eastin, for your continued support and expertise in this research and making it better every step of the way. To my officemates, you all pushed me to become a better meteorologist and I am so grateful for that along with a lifetime of memories and friendships. To my family, as the single greatest joy in my life, I thank each and every one of you for your support and love as I embarked on this journey. Lastly but most importantly, I thank God each and every day for his love and blessings that I receive as a constant reminder of his glory.

TABLE OF CONTENTS

LIST OF TABLES

LIST OF FIGURES

CHAPTER 1. INTRODUCTION

Severe weather, a significant event that occurs throughout the year but particularly in the springtime across the United States, can cause millions of dollars in property and agricultural loss, as well as serious injury or death. Ordinary thunderstorms are quite common, with around 100,000 each year in the United States; of these, about 10,000 become severe (NSSL 2012). Even more rare are the development of supercell thunderstorms, with tornadogenesis being a concern, but not common (Trapp et al. 2005). Pinpoint forecasting tornadic formation within supercell thunderstorms is a rigorous task due to the likelihood of rotation at the lower levels (Markowski et al. 2011). While the physical and dynamical processes of supercell thunderstorms have been researched thoroughly in previous studies (Rotunno and Klemp 1985; Rotunno 1993; Thompson et al. 2003), predicting tornadogenesis remains a challenge. Indeed, two extensive prior field studies have been devoted to learning about tornado dynamics and tornadogenesis: the first and second Verification of the Origins of Rotation in Tornadoes Experiment (VORTEX and VORTEX2; Rasmussen et al. 1994; Wurman et al. 2012) have gathered crucial research observations for understanding these types of events.

The second Verification of the Origin of Rotation in Tornadoes Experiment (VORTEX2; Wurman et al. 2012) in 2009 and 2010 allowed researchers to utilize soundings (among a myriad of other observation platforms) to study a number of dynamical properties of tornadogenesis and supercell thunderstorms. The platform as seen in Figure 1 displays a select number of observational instruments used during the VORTEX2 project (Wurman et al. 2012). The general environment that tornadoes form in is fairly well understood (e.g., Rasmussen and Blanchard 1998; Rasmussen 2003), but

spatial and temporal variability in the environment can be important in determining tornadogenesis (e.g., Markowski et al. 1998; Rasmussen et al. 2000; Wurman et al. 2012). Notably, sounding measurements that have led to numerous tornado forecasting parameters are not taken from during the duration of a supercell, instead taken sometimes several hours before the tornado was observed. However, VORTEX2 launched numerous soundings throughout the lifetime of each supercell within the near storm environment (Wurman et al. 2012; Parker 2014). This provides a valuable opportunity to examine the temporal evolution of the near-storm environment before and after tornadogenesis (or tornadogenesis failure).

With this in mind, the focus of this research is on the temporal evolution of the inflow environments of 34 supercell thunderstorm events observed during the VORTEX2 field study. Comparisons of tornadic and non-tornadic supercells are administered to further understand the complexities of the environmental change as seen in studies such as Klees et al. (2016) allowing for more focus on improving the forecasting of these mesoscale events. Statistical analysis of the comparisons of inflow sounding parameters related to these particular storms will allow for more advancement of forecasting capabilities with supercell thunderstorms. The overall goal in this continuing process of researching supercell thunderstorms and tornadoes associated with these storms is an enhanced understanding and grasp on the potential for forecasting these events in a faster and more precise amount of time to increase awareness and mitigation for those being affected.

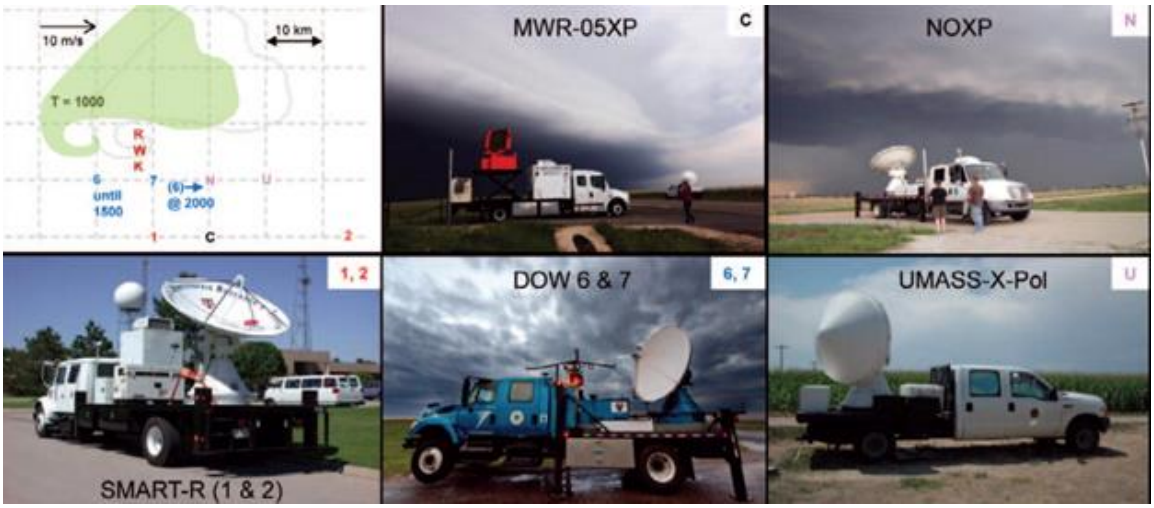

Figure 1. From Wurman et al. (2012), a graphical guidance of platforms used during the VORTEX2 project. Dual Doppler and mesocyclone radars present with a typical storm scale deployment graphic.

CHAPTER 2. BACKGROUND

2.1 Supercell Dynamics

With the commonality of ordinary thunderstorms, it is understandable our knowledge of supercell thunderstorms has been an evolving process throughout the last 40 years allowing for comprehensive analysis for such a dangerous event. The Thunderstorm Project (Byers and Braham 1949) was one of the first studies performed on the structure of ordinary thunderstorms which paved way to the eventual discovery and continued research of supercell thunderstorms. Over the course of the last half-century researchers have developed an understanding of the governing processes in supercells and serves as the basis for supporting the process of tornadogenesis (Lemon and Doswell 1979; Klemp and Rotunno 1987; Rotunno 1993; Thompson et al. 2003).

There must be ideal conditions for the development of mature supercells, with a number of environmental parameters providing useful guidelines. Atmospheric instability (quantified as convective available potential energy; CAPE) values typically greater than 1000 J/kg are supportive of strong updrafts in supercells (Rasmussen and Blanchard 1998; Rasmussen 2003; Davies-Jones 2015). Surface-based CAPE (SBCAPE) in particular has proven to be useful for supercell classification and tornadogenesis due to focus on the buoyancy of low-level parcels to ensure elevation to their levels of free convection (LFCs; Klemp and Rotunno 1983; Rasmussen 2003). SBCAPE provides more representation of convection at the lower levels than most-unstable or mixed-layer CAPE (MUCAPE or MLCAPE) which allows for more confidence in forecasting heavy wind events such as tornadoes (Bunkers et al. 2002). MUCAPE does provide information on the presence of any elevated instability, particularly when its value is larger than

MLCAPE or SBCAPE (Rasmussen and Blanchard 1998; Bunkers et al. 2002; Davies-Jones 2015). Convective inhibition (CIN) values can hint at the potential for surface-based versus elevated convection. For example, when SBCIN is large, an existing supercell could weaken, or in fact be maintained if both MUCAPE is sufficient and there is minimal MUCIN.

The most understood contrast between supercells and other types of thunderstorms deals with the formation and maintenance of a mesocyclonic region within the updraft (Brandes 1978; Markowski and Richardson 2010). Once an updraft forms in an environment with sufficient CAPE and minimal CIN, large vertical wind shear is pivotal to the development and evolution of the supercell. With strong vertical wind shear, supercells can maintain a greater strength (Lemon and Doswell 1979; Bunkers et al. 2006a; Ziegler et al. 2010; Coffer and Parker 2015). Streamwise vorticity becomes pivotal for the formation of the mesocyclone region with the inclusion of tilted vertical wind shear thus becoming embedded in the updraft region (Davies-Jones 1984, Weisman and Rotunno 2000). Typically, long-lived supercells go through environments with 0-8 km bulk shear values of 20 m/s to 40+ m/s (Markowski et al. 2003; Bunkers et al. 2006a, b; Coffer and Parker 2015).

The development of the rotating updraft is first introduced with a vorticity couplet which is derived from the environmental horizontal vorticity vector tilting mechanism (Fig 2; Markowski and Richardson 2010). Streamwise vorticity is present if the direction of the storm motion and the horizontal vorticity vector is the same (Fig 3; Markowski and Richardson 2010). With the utilization of the vertical wind shear tilt along with the streamwise vorticity, the vertical vorticity vector will be parallel to the updraft motion

and allow for rotation creating the mesocyclone (Markowski and Richardson 2010). Helicity plays an important role in the updraft rotation process being that it is influenced by streamwise vorticity with values of higher helicity generally be developed from streamwise vorticity (Markowski and Richardson 2010). Storm relative helicity (SRH) is the environmental helicity values which in turn have an influence on the sign (+/-) depending on the vorticity (streamwise or anti-streamwise) (Markowski and Richardson 2010).

Particularly for cases where surface-based instability is limited, it is helpful to examine shear and SRH over layers that are not fixed depths. The effective layer is defined as the layer in which CAPE is greater than 100 J/kg and CIN is less than 250 J/kg (Thompson et al. 2007). Importantly, effective SRH (ESRH) was found to be useful and discriminatory when comparing tornadic and non-tornadic supercells (Thompson et al. 2007). Effective Bulk Shear (EBS) was found to be just as effective as 0-6 km shear when distinguishing between supercell and ordinary/multicell storms. The effective layer will prove to be pivotal in this research so that assessing the parameters will be solely based around the environmental inflow region especially in the case of elevated supercells.

2.2 Supercell Tornadogenesis

With the majority of strong tornadoes being associated with supercell thunderstorms, it is a more developed process of forecasting these events within supercells versus the opposite (Klemp and Rotunno 1983; Trapp et al, 2005a; Markowski and Richardson 2009; Davies-Jones 2015). Tornado formation generally occurs an hour after the storm has begun developing into the mature stage (Davies-Jones 2015). Note

that the presence of lower-level rotation (i.e., a low-level mesocyclone) alone is not sufficient for tornadogenesis to occur (Markowski and Richardson 2009; Wurman et al. 2012; Davies-Jones 2015). Even so, a low-level mesocyclone is an important component in indicating that there is an intense updraft tilting and stretching of environmental vorticity into the vertical. The key is in how to get that vorticity down to the surface to produce a tornado. Downdrafts are an essential part of the process because they are useful in moving vertical vorticity down to the surface especially when rotation is previously absent near the surface (Fig 4; Markowski and Richardson 2010; Wurman et al. 2012). The rear flank downdraft plays a pivotal role in the formation of these tornadoes but by different means of processes on a case by case basis (Wurman et al. 2012).

2.3 Tornado Forecasting

Forecasting tornadogenesis remains a challenge, but there are parameters that have been demonstrated to be useful, including water vapor concentration in the boundary layer in reference to relative humidity and vertical wind shear just above ground level (Markowski and Richardson 2009; Parker 2014; Coffer and Parker 2017). Relative humidity and vertical wind shear at the lower level may prove to be efficient in relating tornadic versus non-tornadic supercell (Markowski and Richardson 2009). The depth of the source of moisture in the boundary layer may be influenced when the two parameters are enhanced especially with the inclusion of a convergence zone as described in Markowski and Richardson (2009). Low level horizontal vorticity can be increased from baroclinic vorticity along boundaries associated with mesoscale events in particular (Markowski and Richardson 2009). This in turn would be a beneficial set of parameters

to look at using the VORTEX2 dataset for further evaluation and examine the comparisons and contrasts of tornadic and non-tornadic supercells.

2.4 Environmental Variability

It is well-understood that environmental variability (i.e., spatiotemporal gradients in thermodynamic and kinematic quantities) impacts supercell intensity and evolution, thus impacting severe weather production and tornadogenesis. This has been demonstrated in a few ways in the VORTEX2 dataset (Parker 2014, Davenport and Parker 2015a, Davenport and Parker 2015b). For example, Parker (2014) created spatial composites of the environment surrounding well-observed supercells based on a larger number of soundings collected in the vicinity of each storm as seen in Figure 5.

Notably, there were enhanced levels of buoyancy instability, vertical shear, and relative humidity in tornadic events (Fig 6; Parker 2014). There were also differences in the environment surrounding a storm early versus late in its life, largely tied to the diurnal cycle (Fig 7, Parker 2014). There is also an agreement with supercell composite parameter and significant tornado parameter values taken in Parker (2014) that has an overall accuracy to the dataset used.

Parker (2014) acknowledges the fact that using one sounding to represent the environmental inflow is not an efficient process because of storm motion and a heterogeneous environment resulting in constant changing of parameter values. This is where this research becomes pivotal in understanding the inflow environmental changes throughout the course of the supercell from the initial sounding launch to the last resulting launch. Use of this process will be helpful with understanding the temporal evolution of these parameters and the dynamical processes associated with the constant

changing within the supercell. One particular suggestion in Parker (2014) is that there is a lot to information that is crucial for analyzing the near storm environment by observing the inflow region within 75 kilometers, there are similarities in the soundings with reference to near and far inflow regions, though the wind profile tends to be slightly more favorable in the near inflow environment (Fig 8; Parker 2014).

Davenport and Parker (2015a) and Davenport and Parker (2015b) takes an approach at understanding the dynamical changes within a dissipating supercell observed during the same dataset present for this research. In particular to the inflow region of the supercell, they found that the inflow environment had sufficient CAPE for storm maintenance, while also exhibiting increases over time in low-level CIN. Even so, the elevated environment became more favorable, with decreases in CIN (Fig. 9). Deep-layer shear and SRH also evolved over time, which were hypothesized to influence the strength of dynamic lifting of low-level parcels, thus leading to demise. After testing these thermodynamic and kinematic changes in a series of idealized modeling experiments using base-state substitution modeling technique (Letkewicz et al. 2013), Davenport and Parker (2015b) found that the thermal variations with the updraft region of the parcel were a major contributing factor to supercell demise.

Klees et al. (2016) also demonstrated the impact of environmental variability on supercells; this study compared two supercells in close proximity of the other, where one became tornadic while the other was non-tornadic. The goal was to identify any contrasts in the data to tell why the non-tornadic supercell did not produce a tornado. One big difference was the interaction in how the supercells interacted with the parent cell. Spatial variability in storm-relative helicity at the lower levels also proved to be a key factor in

comparing the two supercells as there were lower values in the non-tornadic event as seen in Figure 10; image b. Temporal variations were discussed due to the fact that the tornadic storm had more time to be isolated and keep its supercellular structure allowing for tornadogenesis to arise. The tornadic storm also experienced a more enhanced rotation at the lower levels allowing for better chances of tornadogenesis.

An important source of temporal environmental variability is the diurnal cycle, particularly the nocturnal transition and the development of the low-level jet. This feature in the Great Plains significantly enhances low-level shear and SRH, which has a marked impact on supercells. For example, Coffer and Parker (2015) demonstrated using a series of idealized experiments that increasing low-level shear resulted in strong increases in low-level vertical vorticity, thus enhancing dynamic lifting by the mesocyclone near the surface, consistent with observations of enhanced frequency of tornadogenesis near sunset. This is also in line with observations of supercell evolution during the nocturnal transition; Gropp and Davenport (2018) found that increases in SRH and low-level shear were instrumental in supporting supercell maintenance versus dissipation. Having minimal increases in the magnitude of MUCIN was also key in supporting sustained convection. The nocturnal transition may prove to be an important role in understanding the consequences of time with respect to tornadic and non-tornadic events discussed in this research.

Previously researched dynamics and functions of supercell thunderstorms both tornadic and non-tornadic gives us great groundwork to build on the ideas and motivations behind more enhanced forecasting techniques relative to this mesoscale phenomenon. With this in mind, our focus is on filling some of the gaps of what has been

previously researched. In particular, the temporal evolution of these supercell storms has been far less researched versus spatial. By knowing what to expect out of the supercell itself with its various stages, we must then be able to use these associated parameters to enhance our level of understanding for when tornadogenesis may occur. The majority of the previous research on tornadogenesis views mesocyclonic tornadogenesis as a forefront for what needs to be researched most especially with respect to time. This new approach towards the temporal evolution of parameters associated with these storms may add a more concrete and faster method of identifying the potential for tornadoes within supercell thunderstorms.

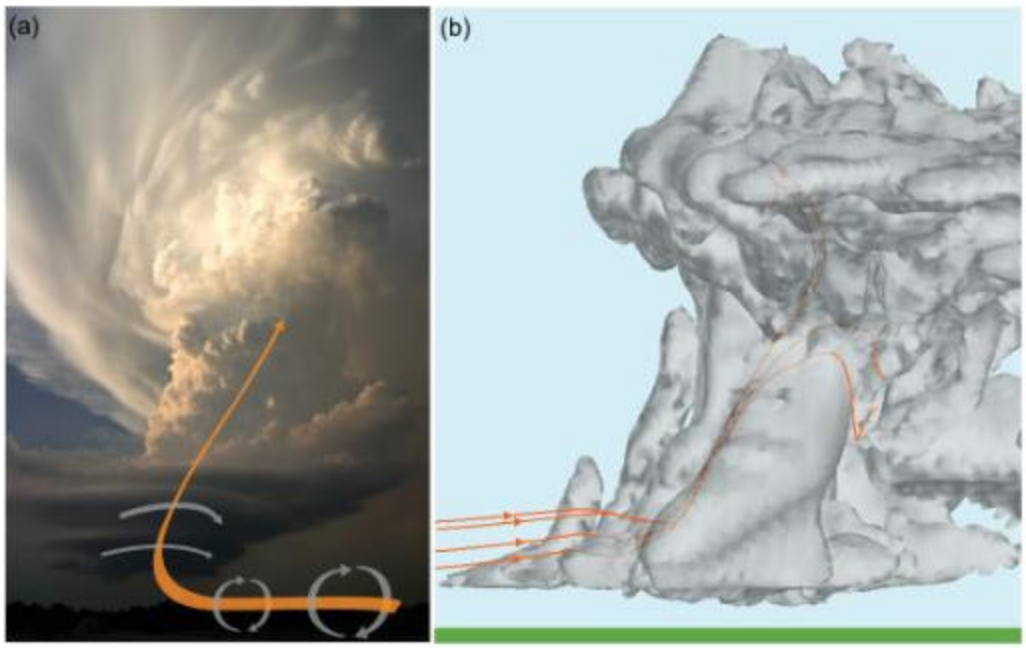

Figure 2. From Markowski and Richardson (2010):, image (a) is a vertical profile of vertical vorticity as it is tilted from the effects of horizontal vorticity and vertical shear. Image (b) is a simulated profile of the development of the updraft.

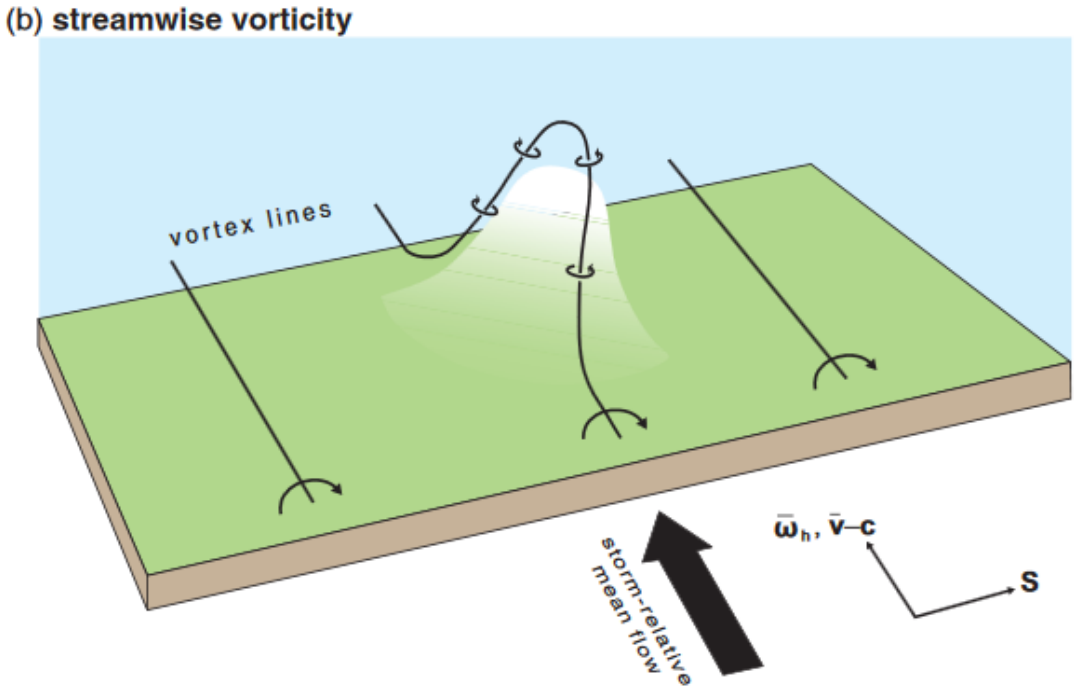

Figure 3. From Markowski and Richardson (2010), demonstrating streamwise vorticity formation and structure.

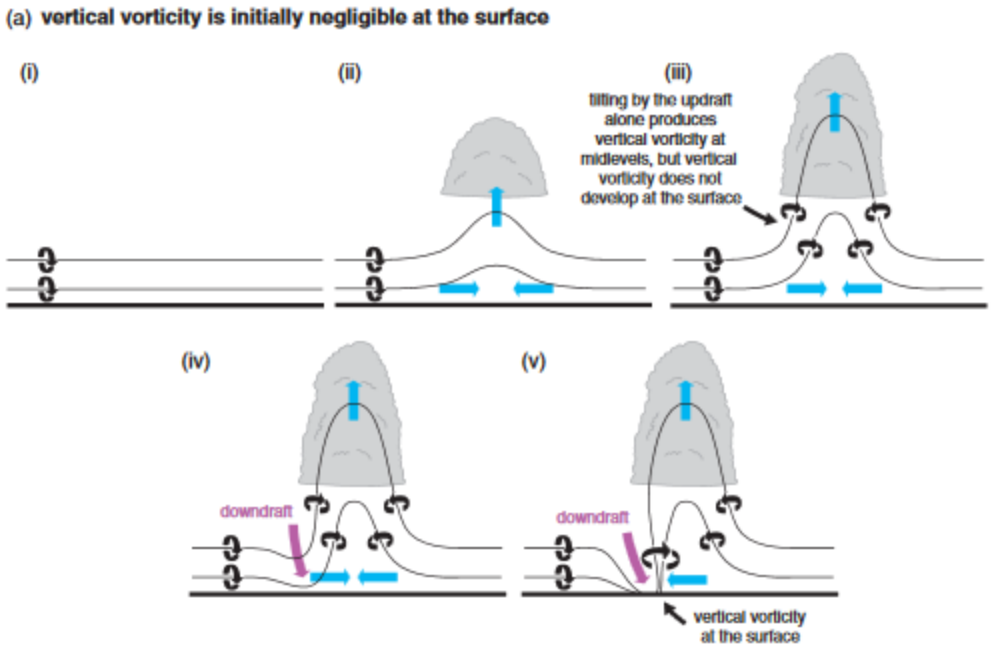

Figure 4. From Markowski and Richardson (2010): Illustration of creation of strong vertical vorticity at the surface where there is lack of pre-existing vertical vorticity at the surface; the downdraft plays a critical role for supercell tornadogenesis.

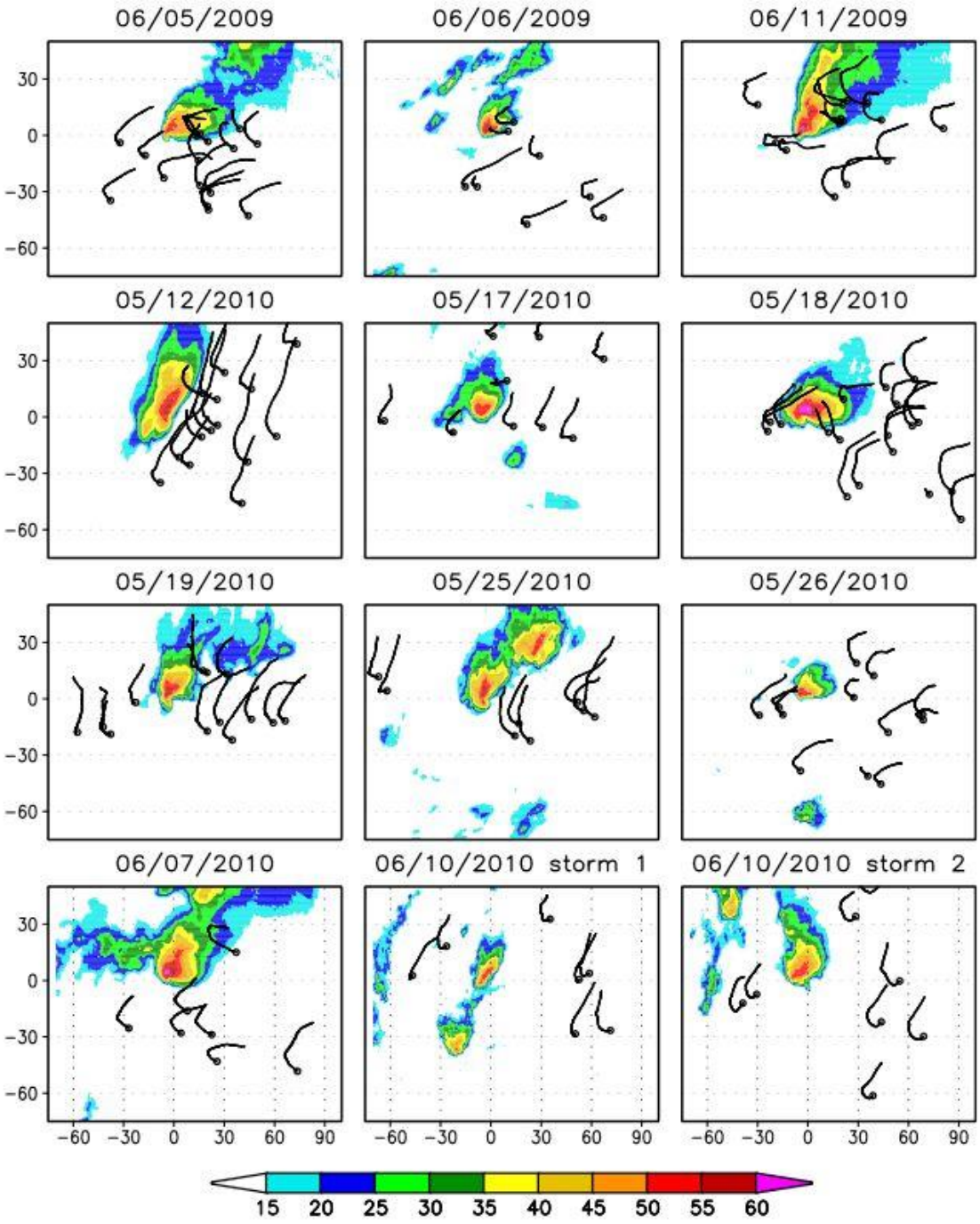

Figure 5. From Parker (2014): Storm-relative sounding launch paths and positions.

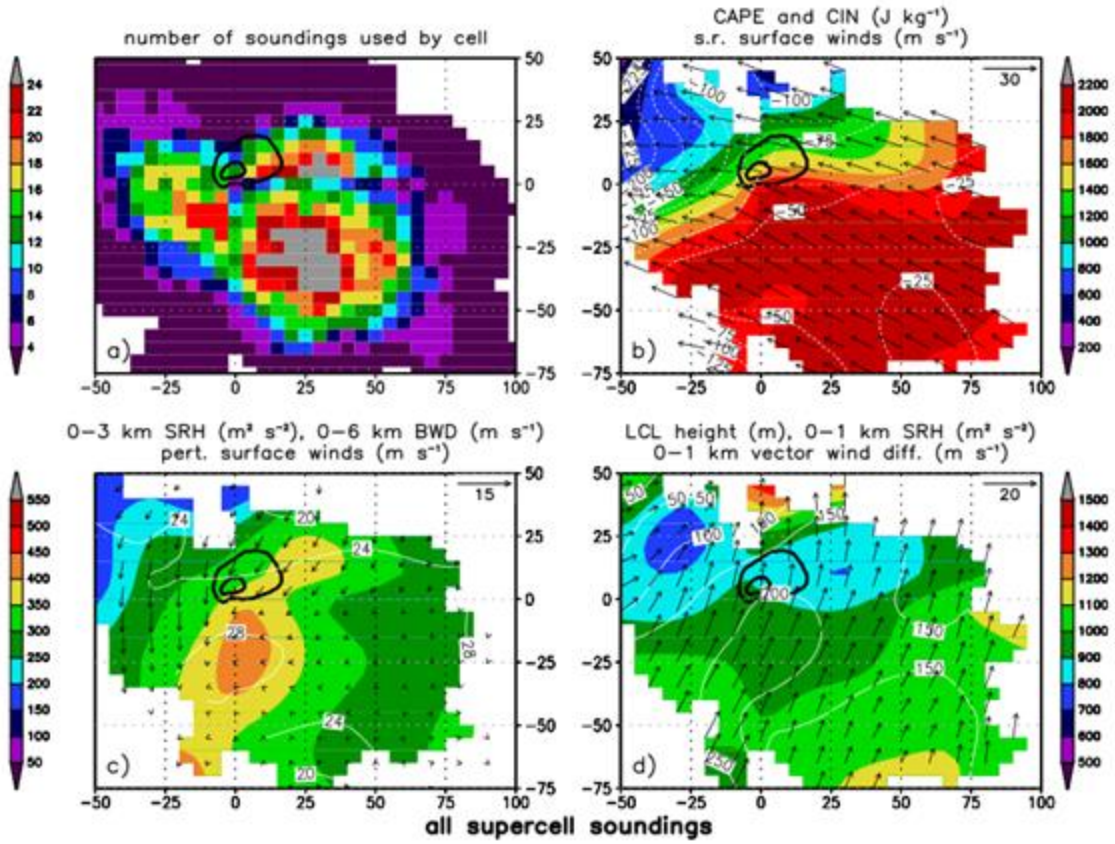

Figure 6. From Parker (2014): A composite analysis of all 134 supercell soundings with the following shaded quantities: number of soundings in each grid cell (upper left), instability and inhibition (upper right), low-level storm-relative helicity (lower left) and lifted condensation levels (lower right).

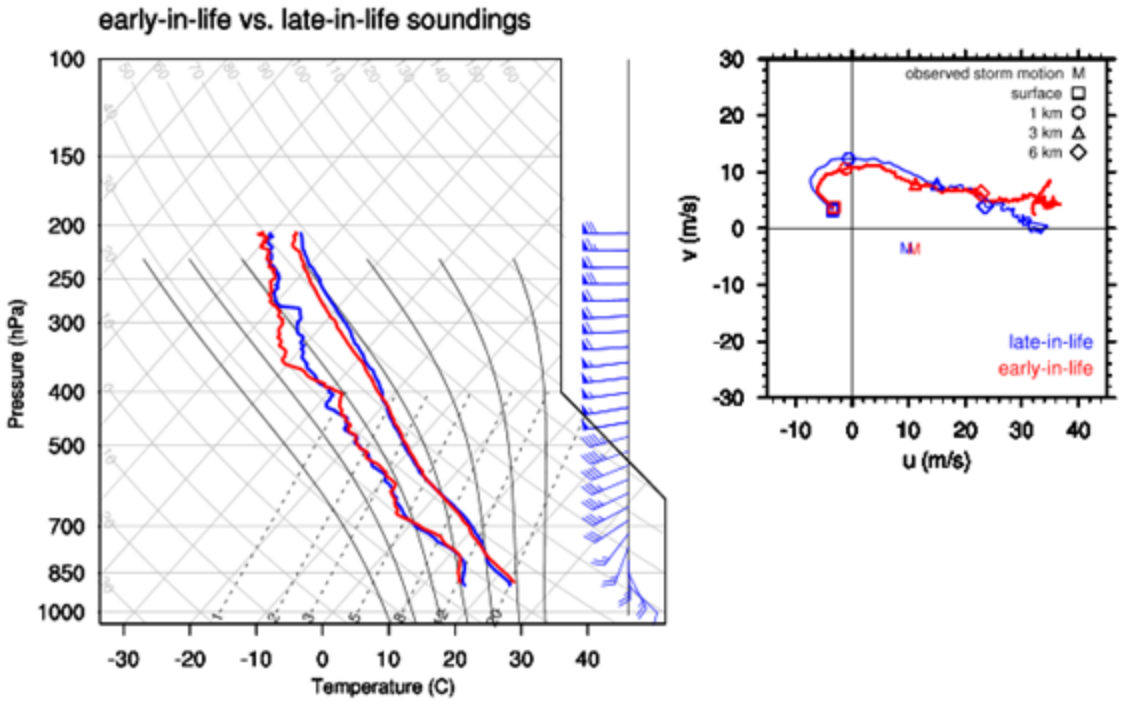

Figure 7. From Parker (2014): Composite profiles of early in life soundings (red) vs. late in life soundings (blue), along with accompanying hodographs.

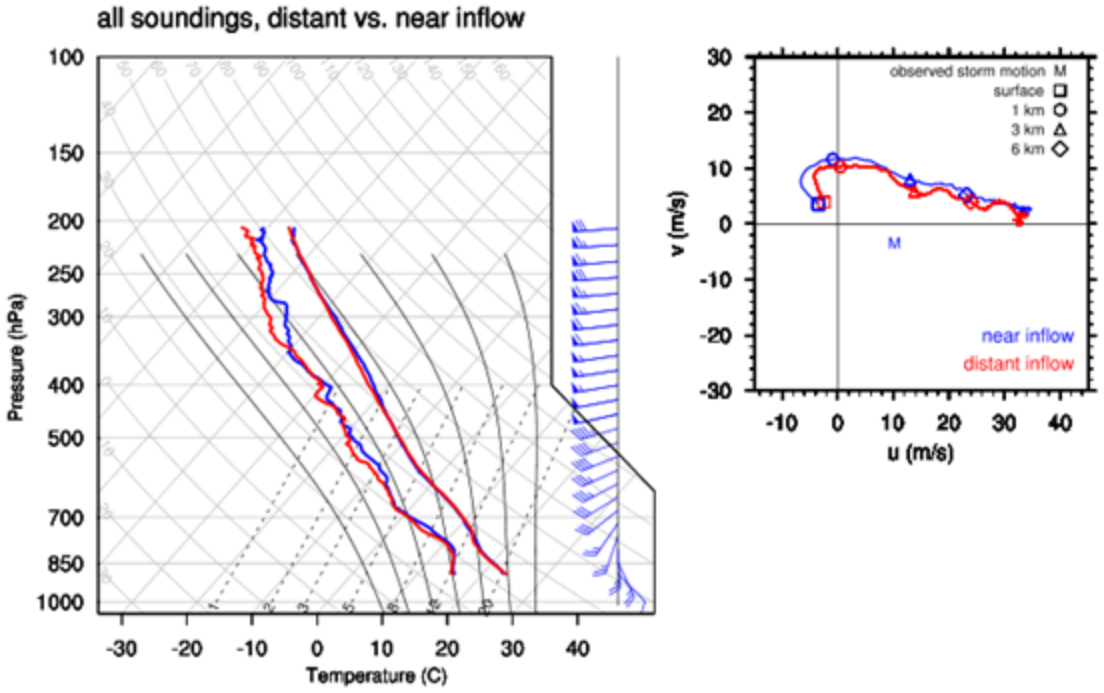

Figure 8. From Parker (2014): Composite sounding profiles of near (blue) and far (red) inflow launch locations, along with accompanying hodographs.

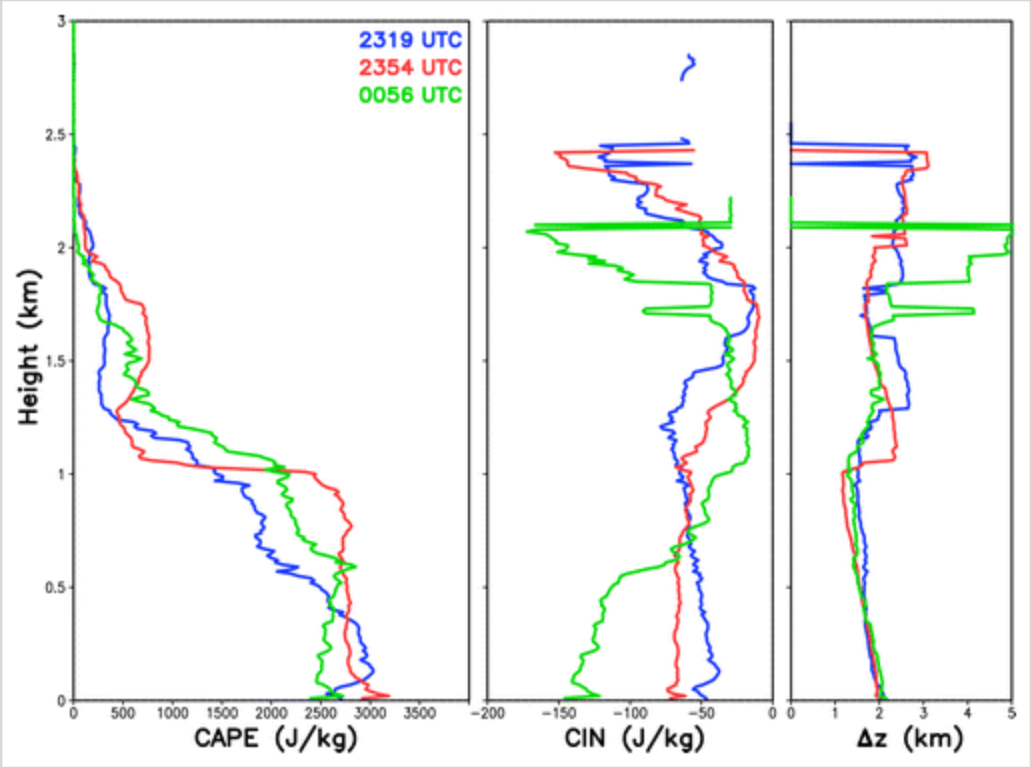

Figure 9. From Davenport and Parker (2015a): Vertical profiles of CAPE, CIN, and vertical distance between a parcel's starting height and its level of free convection (delta-z) for the June 9 2009 VORTEX2 supercell.

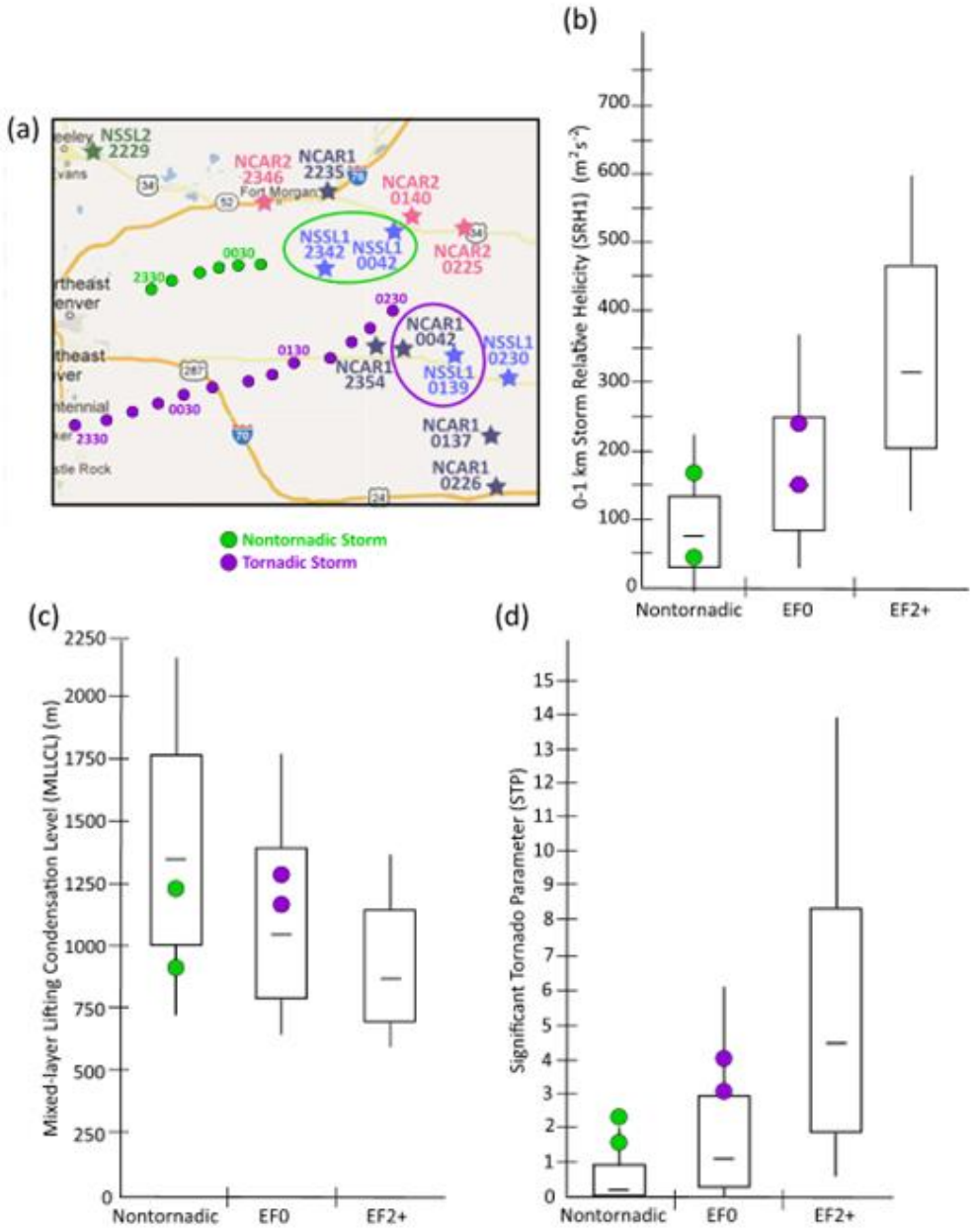

Figure 10. From Klees et al. (2016): (a) Map representing the location of sounding deployments with the dots representing the location of the midlevel mesocyclone. (b-d) is three parameters used for comparison of the non-tornadic storm and the tornadic storm along with a normal EF2+ range of values for a tornado of that strength.

CHAPTER 3. DATA AND METHODOLOGY

3.1 VORTEX 2 Soundings

The goal of this research is to measure the environmental changes over time in the inflow region of tornadic and non-tornadic supercell thunderstorms to determine any relationship between observed environmental shifts and the potential for tornadogenesis. This goal is being accomplished by leveraging the VORTEX2 sounding observations. All of the soundings were made with Vaisala RS92 radiosondes. The soundings were launched by field scientists working with the VORTEX2 project and they precisely released and observed through various sections of the storm. Ideally, launches occurred in the rear-flank outflow, near and far (distant) inflow and forward flank regions (Fig 2; Parker 2014). Distances from each actual region and area of release were dependent upon safe proximity to the storm as well as logistical considerations such as road options. Data were later quality controlled by the National Center for Atmospheric Research Earth Observing Laboratory (NCAR EOL; details explained on the EOL VORTEX2 archive: http://data.eol.ucar.edu/master_list/?project=VORTEX2).

For the purposes of this study, only supercellular events sampled by VORTEX2 were examined; each supercell sampled was counted as its own event. Next, each event was observed to see if the number of soundings would be appropriate for the analysis. Given the focus on the temporal evolution of the inflow environment, only events that had *at least* three inflow soundings (majority being near-inflow) were included in this study's dataset. This resulted in a total of 114 soundings over 38 supercell events (11 tornadic, 27 non-tornadic), listed in Table 1. Each sounding was transferred from the .eol format into a .csv format so that the resulting data could be ingested into the Python

library SharpPy (Blumberg et al. 2017). All of the parameters chosen for calculation were commonly-used forecasting parameters, conducted using SharpPy. They include atmospheric buoyancy, shear, helicity and various levels of atmospheric importance (LCL, LFC, EL). The buoyancy parameters (CAPE, CIN) were calculated at surface, mixed and most unstable layers of the profile. The parameters as seen in Table 2 include the various layers of the atmosphere pivotal to supercell maintenance and tornadogenesis.

3.2 Time Series Analysis

Each event was broken down with each parameter value for the three or more inflow soundings and made into a time series. For the tornadic events, the time series will include observed times of peak tornadogenesis and tornado dissipation. The time series is used to show the evolution of the parameters over the course of the supercell event in the inflow region. The goal is then to examine the change in the characteristics of the inflow environment over time to determine any differences between tornadic and non-tornadic supercells. Importantly, any changes right before or after tornadogenesis/dissipation will help to pinpoint key processes that can aid or inhibit tornado production.

For ease of comparison with the non-tornadic cases each of the non-tornadic supercell cases were analyzed to find the peak time of low-level mesocyclone intensity. The times were observed by using WSR-88D radar imagery scans from the National Weather Service using the Weather and Climate toolkit as well as the provided VORTEX2 radar scans done by a number of the observing mobile radars seen in Figure 1. Using the radar radial velocity measures once a mesocyclone was detected along with a mesocyclone recognition nomogram the peak low-level mesocyclone intensity time was observed. Each scan during each available time was observed for proper noting of the

specific time of maximum meso intensity. While performing this task, an observation was made of the closest distance to a surface boundary relative to the location and time of peak mesocyclone intensity or tornadogenesis (Table 3).

With this, a distribution of each parameter is made (tornadic and non-tornadic) by making a violin plot using MetPy program to configure the correct distributions of the dataset. Another way of visualizing the parameters was through normalizing the dataset with respect to time of tornadogenesis or maximum low-level mesocyclone intensity as well as sunset times. This step is key due to the nonlinear times of balloon launches relative to each case.

3.3 Statistical Analysis

The dataset (tornadic and non-tornadic) were taken and run through a two-sample comparison of means t-test between all the tornadic and non-tornadic parameter values (i.e., regardless of when data point was collected with respect to tornadogenesis or maximum mesocyclone intensity) to test if the parameters associated with the dataset were statistically significant using a standard p-value of 0.05 for reference. Once the statistical significance test is performed, the statistically significant parameter values are then included in a scatter plot relative to tornadogenesis or peak low-level mesocyclone intensity and local sunset. Using multiple regression models help with testing how changes in the two or more predictor variables are able to properly predict how much change occurs with the outcome variable. This in turn would allow us to focus on the parameters that are statistically significant to the dataset especially with respect to the tornadic supercells for enhanced understanding on prediction of the events.

Table 1. Supercell event dates and times (in UTC) of first three inflow soundings for both tornadic (red) and non-tornadic (blue or white) supercells.

Event Date	1st inflow sounding	2nd inflow sounding	3rd inflow sounding
5/13/2009	23:24	23:32	0:34
5/20/2009	22:00	22:15	0:05
5/25/2009	23:36	23:39	23:47
5/26/2009	0:32	0:54	1:05
5/29/2009	1:05	1:43	1:48
6/4/2009	23:03:25	23:03:29	23:05:27
6/4/2009	23:08:35	23:55	0:43
6/5/2009	21:55	22:40	23:35
6/6/2009	23:03	23:05	23:45
6/6/2009	1:13	1:19	1:21
6/7/2009	22:58	23:45	23:48
6/9/2009	23:06	23:19	23:44
6/11/2009	23:16	23:17	23:21
6/11/2009	15:18	15:20	15:46
5/6/2010	0:39	1:06	1:17
5/10/2010	19:56	20:57	21:45
5/11/2010	23:11		
5/11/2010	1:09	1:25	
5/12/2010	23:02	0:16	1:30
5/14/2010	18:30	19:26	20:00
5/17/2010	20:44	22:04	22:50
5/18/2010	22:16	22:56	23:40
5/19/2010	21:00	21:54	22:57
5/21/2010	0:25	0:33	1:29
5/23/2010	0:21	0:43	1:24
5/24/2010	19:19	20:29	21:18
5/25/2010	22:27	23:26	0:33
5/26/2010	21:09	22:23	23:20:40
6/2/2010	23:10	23:13	23:16
6/3/2010	23:40	28:49:00	1:21
6/6/2010	22:10	22:56	23:49
6/6/2010	1:07	1:18	1:27
6/7/2010	23:41	0:35	0:40
6/7/2010	1:40	1:44	2:25
6/9/2010	0:45	1:13	1:15
6/10/2010	23:42	0:42	1:38
6/11/2010	23:41	1:12	1:15
6/12/2010	20:12	21:26	21:48
6/13/2010	20:45	22:03	23:09
6/14/2010	19:56	20:04	20:22

Table 2. Parameters used in this research along with associated units.

Parameter Name	Units
SBCAPE	J/kg
SBCIN	J/kg
MUCAPE	J/kg
MUCIN	J/kg
0-1 km SRH	m^2/s^2
0-3 km SRH	m^2/s^2
ESRH	m^2/s^2
STP (fixed)	
SCP	
EBWD	m/s

Table 3. Case Details for each supercell event with date, type, EF-Scale and closest proximity to a surface boundary (km).

Date	Type of Event	EF-Scale (if applicable)	Proximity to surface boundary (km
6/5/2009	Tornadic Supercell	2	116
5/10/2010	Tornadic Supercell	3	112
5/10/2010	Tornadic Supercell	3	77
5/12/2010	Tornadic Supercell	1	41
5/14/2010	Tornadic Supercell	3	55
5/18/2010	Tornadic Supercell	2	66
5/18/2010	Tornadic Supercell	1	75
5/19/2010	Tornadic Supercell	1	74
5/25/2010	Tornadic Supercell	0	38
6/7/2010	Tornadic Supercell	1	132
6/13/2010	Tornadic Supercell	0	87
6/7/2010	Tornadic Supercell	1	125
6/10/2010	Tornadic Supercell	1	97
6/11/2010	Tornadic Supercell	0	145
5/13/2009	Non-Tornadic Supercell		370
5/20/2009	Non-Tornadic Supercell		187
5/25/2009	Non-Tornadic Supercell		203
5/26/2009	Non-Tornadic Supercell		39
5/29/2009	Non-Tornadic Supercell		238
6/4/2009	Non-Tornadic Supercell		437
6/6/2009	Non-Tornadic Supercell		67
6/7/2009	Non-Tornadic Supercell		164
6/9/2009	Non-Tornadic Supercell		28
6/11/2009	Non-Tornadic Supercell		176
5/6/2010	Non-Tornadic Supercell		65
5/11/2010	Non-Tornadic Supercell		29
5/17/2010	Non-Tornadic Supercell		154
5/21/2010	Non-Tornadic Supercell		97
5/23/2010	Non-Tornadic Supercell		89
5/24/2010	Non-Tornadic Supercell		85
5/26/2010	Non-Tornadic Supercell		78
6/2/2010	Non-Tornadic Supercell		197
6/3/2010	Non-Tornadic Supercell		156
6/6/2010	Non-Tornadic Supercell		114
6/6/2010	Non-Tornadic Supercell		106
6/9/2010	Non-Tornadic Supercell		221
6/12/2010	Non-Tornadic Supercell		102
6/14/2010	Non-Tornadic Supercell		85

CHAPTER 4. RESULTS

The supercells in discussion here were analyzed and compared based off of their associated parameters with a temporal scale-based analysis. We want to know if the temporal scale associated with these storms has a significance to the overall maintenance of these supercells along with understanding more about mesocyclone tornado forecasting. The distribution of these parameters are represented over the first three inflow soundings in the sounding launch process performed during VORTEX2. The times of the soundings vary within the distribution as they are the entire dataset with the average times of the 1st-3rd soundings being 22:57:55 UTC, 23:09:51 UTC and 23:45:41 UTC respectively. The parameter subsections are broken down to show comparisons of the distributions between the first three soundings, comparing the distributions relative to tornadogenesis or peak mesocyclone intensity and sunset as well as displaying the results of the statistical tests performed which can be seen in Table 4.

4.1 SBCAPE

The average surface-based CAPE values experienced a constant decline throughout the first three soundings in the tornadic cases with a slightly larger decrease after the 2nd sounding as seen in Figure 11. The non-tornadic cases had an average decrease from the 1st to 2nd sounding while experiencing an increase going from the 2nd to the 3rd sounding. With Figure 12 showing the violin distribution of SBCAPE, one is able to see the means visually for all three soundings as well as where the distribution for each sounding and case type is positioned. A few key points for this particular parameter is that there is a larger distribution with the 1st sounding for the tornadic events with the smallest distribution being the 2nd sounding for the non-tornadic events.

Additionally, consistent with the time series of the mean values, tornadic cases tend to exhibit larger SBCAPE values than non-tornadic cases, as exhibited by comparing the CAPE values aligned with the widest portion of the violin plots; these higher CAPE values may help to promote stronger tilting and stretching of vorticity, supporting tornadogenesis. However, relative to the time of tornadogenesis or peak mesocyclone intensity, there is no clear trend aside from a general decrease in SBCAPE values over time (Fig. 13), likely related to the nocturnal transition. Indeed, parameter values relative to the time of sunset do demonstrate a general downward trend, though there is a subset of cases where SBCAPE appears to increase slightly in the couple of hours right before sunset (Fig. 14). From Table 4, one can see that SBCAPE did not appear to have statistical differences between tornadic and non-tornadic events with a two-sided p-value of 0.0922, greater than the threshold of 0.05 for statistical significance.

4.2 SBCIN

The time series of average SBCIN shown in Figure 15 shows a similar trend with both the tornadic and non-tornadic cases, in that there is a slight decrease in the magnitude between the first and second sounding, followed by a large increase in magnitude between the second and third sounding. Overall, the broader distributions are similar for the first and second soundings, while the third sounding shows a much larger range for non-tornadic cases (Fig 16). Relative to the time of peak mesocyclone intensity and tornadogenesis, there does not appear to be a clear trend (Fig. 17). Unsurprisingly, relative to sunset, SBCIN tends to increase as the day wears on due to cooling of the low-level environment (Fig. 18). From Table 4, one can see that SBCIN did not appear to

have statistical differences between tornadic and non-tornadic events with a two-sided p-value of 0.535, greater than the threshold of 0.05 for statistical significance.

4.3 MUCAPE

Evolution in most-unstable CAPE was largely similar to the evolution in SBCAPE. For example, the tornadic events displayed a slight decrease on average between the 1st sounding to the 2nd sounding, followed by an increase (Fig. 19). This pattern is also largely reflected in the distribution of values for each sounding (Fig. 20). Relative to the time of tornadogenesis or max mesocyclone intensity, there is much overlap in the distribution, however the tornadic cases tend to have higher MUCAPE values than the non-tornadic cases, and sustain those higher values post tornadogenesis as well (Fig. 21). Notably, however both tornadic and non-tornadic cases exhibit similar temporal trends relative to the time of sunset (Fig. 22). From Table 4, one can see that MUCAPE did appear to have statistical differences between tornadic and non-tornadic events with a two-sided p-value of 0.0236, less than the threshold of 0.05 for statistical significance.

4.4 MUCIN

As shown in Figure 23, on average, non-tornadic events tended to exhibit stronger MUCIN values; while the first sounding average had less MUCIN for non-tornadic events, there was a steep increase between the first and second soundings. This trend is further evident in the distributions of all MUCIN values, where non-tornadic cases more frequently contain higher MUCIN magnitudes, as well as larger ranges (Fig. 24). Near the time of tornadogenesis, there is much overlap between the tornadic and non-tornadic cases, yet there is a slightly stronger cluster of tornadic cases with smaller MUCIN

magnitudes; non-tornadic cases, in contrast, simply exhibit a large range of values near the time of peak mesocyclone intensity (Fig. 25). Relative to sunset, MUCIN generally increases for both tornadic and non-tornadic cases as the nocturnal transition occurs, with no clear differentiation between event types (Fig. 26). From Table 4, one can see that MUCIN did not appear to have statistical differences between tornadic and non-tornadic events with a two-sided p-value of 0.545, greater than the threshold of 0.05 for statistical significance.

4.5 0 to 3 km SRH

Average 0-3 km SRH values, indicative of potential for the environment to support rotating updrafts, increase over time throughout the entire duration of the first three inflow soundings in both tornadic and non-tornadic cases, likely a result of the development of the Great Plains low-level jet (Fig. 27). Notably, however, the increases tend to be a bit sharper for tornadic events. Indeed, the full distribution of 0-3 km SRH values in Figure 28 illustrates the more extreme values found in tornadic cases, particularly between the second and third soundings. However, relative to the time of tornadogenesis or max peak mesocyclone intensity, there is much overlap in the SRH values, with no clear visual separation between case types (Fig. 29). The significant overlap is also evident with respect to the time of sunset (Fig. 30). From Table 4, one can see that 0 to 3 km SRH did not appear to have statistical differences between tornadic and non-tornadic events with a two-sided p-value of 0.6408, greater than the threshold of 0.05 for statistical significance.

4.6 0 to 1 km SRH

Examining 0-1 km SRH values demonstrate more noticeable separation between tornadic and non-tornadic cases, consistent with prior research (e.g., Markowski et al. 1998; Thompson et al. 2007). For example, in Figure 31, tornadic cases clearly have larger 0-1 km SRH values on average than non-tornadic cases, though the overall upward trends are similar. This finding is also clear when examining the broader distributions of tornadic and non-tornadic cases (Fig. 32). Trends in 0 to 1 km SRH relative to tornadogenesis or peak mesocyclone intensity, shown in Figure 33, again shows much overlap, though there is a stronger clustering of lower SRH values for non-tornadic cases near the time of peak mesocyclone intensity, whereas tornadic cases display a larger range. Interestingly, there appears to be no clear upward trends in 0-1 km SRH as a result of the nocturnal transition (Fig. 34). From Table 4, one can see that 0 to 1 km SRH did appear to have statistical differences between tornadic and non-tornadic events with a two-sided p-value of 0.0296, less than the threshold of 0.05 for statistical significance.

4.7 Effective SRH

The effective layer SRH, particularly informative during the nocturnal transition because it only accounts for layers that have parcels with instability that can be lifted (i.e, with smaller CIN values; Thompson et al. 2007; Gropp and Davenport 2018), for the tornadic events displayed an increase throughout the duration of the first three soundings as seen in Figure 35, similar to 0-1 km SRH. The non-tornadic events had a smaller distribution than the tornadic events with the tornadic events exhibiting a sharp increase throughout each sounding (Fig. 36). Indeed, the broader distributions of effective SRH values are quite similar to 0-1 km SRH distributions (cf. Figs. 32 and 36). There are not any strong trends in effective SRH near the time of tornadogenesis or peak mesocyclone

intensity (Fig. 37), though tornadic cases do tend to exhibit stronger increases as sunset approaches (with the exception of some small outliers), while non-tornadic cases have no clear sunset-relative trend (Fig. 38). From Table 4, one can see that Effective SRH did appear to have statistical differences between tornadic and non-tornadic events with a two-sided p-value of 0.0468, less than the threshold of 0.05 for statistical significance.

4.8 MULCL

Most unstable LCL heights were lower on average in the tornadic events versus the non-tornadic events as seen in Figure 39. Previous literature has proven that to be in the case and it is present in this research (Davies 2006). At first LCL height trends in both the non-tornadic and tornadic events were pretty linear from the 1st sounding average to the 2nd, followed by increases to the 3rd sounding. Notably, larger ranges are present in non-tornadic cases, as well as increased frequency of higher LCL heights, which tends to be less favorable for tornado production (Fig. 40). It is known that higher MULCL levels potentially indicate that the storms would be elevated which in turn is less favorable would help in forecasting the potential for tornadogenesis based on the elevated level (Craven et al. 2002; Craven et al. 2004; Nowotarski and Markowski 2016). Even so, there is no strong upward or downward trend immediately before or after the time of tornadogenesis to indicate that the observed cases herein exhibited changes in LCL heights that could contribute to (or take away from) the potential for tornado formation (Fig. 41). The only feature of note near the time of tornadogenesis (peak mesocyclone intensity) is the smaller (larger) range of observed MULCL values, consistent with previous research. With respect to sunset, no clear trends are present in tornadic cases, though non-tornadic cases tend to see a decrease in MULCL heights as sunset

approaches, consistent with a cooling and moistening atmosphere during the nocturnal transition (Fig. 42). From Table 4, one can see that MULCL did not appear to have statistical differences between tornadic and non-tornadic events with a two-sided p-value of 0.0852, greater than the threshold of 0.05 for statistical significance.

4.9 MULFC

On average, MULFC heights slowly increase over time in the tornadic cases, while non-tornadic cases exhibit a sharper increase then slight decrease (Fig. 43). The sharper increase present in non-tornadic cases appears to be tied to the significantly larger ranges in MULFC heights in the second and third soundings, a feature not present in the tornadic cases (Fig. 44). Consistent with the MULCL findings, LFC heights also tended to be lower in the tornadic cases versus the non-tornadic cases. Relative to tornadogenesis, there appears to be a slight decrease in LFC heights between approximately 30 min before and 30 min after (Fig. 45), though whether this is physically significant is unclear. Outside of some outlier values, non-tornadic cases seem to demonstrate a slight increase then decrease in LFC heights immediately before then after the time of peak mesocyclone intensity. No clear temporal trends are present relative to sunset (Fig. 46). From Table 4, one can see that MULFC did not appear to have statistical differences between tornadic and non-tornadic events with a two-sided p-value of 0.0796, greater than the threshold of 0.05 for statistical significance.

4.10 SCP

The supercell composite parameter shows clear differences in the trends of the average values. For example, tornadic cases contain sharp increases on average over time, while non-tornadic cases contain little change between the various soundings (Fig.

47), an observation that also bears out in the broader sounding distributions (Fig. 48). However, the sharp increase in SCP values does not appear to be well-correlated to tornadogenesis, as there is no clear upward trend prior to that time (Fig. 49). SCP does exhibit a stronger trend with respect to sunset, where both tornadic and non-tornadic cases demonstrate increases in SCP as the nocturnal transition approaches, with larger values associated with tornadic cases (Fig. 50). From Table 4, one can see that SCP did not appear to have statistical differences between tornadic and non-tornadic events with a two-sided p-value of 0.064, greater than the threshold of 0.05 for statistical significance.

4.11 Fixed STP

Significant Tornado Parameter (as in Thompson et al. 2007) has similar trends as SCP. Figure 51 shows that the values were larger in the tornadic cases versus the non-tornadic cases while increasing throughout the entire duration in the tornadic cases and increasing then decreasing in the non-tornadic cases. The distribution is higher in the tornadic cases with larger maximum distribution values being present in the 2nd and 3rd soundings (Fig. 52). Notably, the overall trend in tornadic cases is different than non-tornadic cases, in that while there is an increasing trend for both tornadic and non-tornadic events between the 1st and 2nd soundings, tornadic cases continue to see a sharp rise in STP values while non-tornadic cases tend to see a decline. Relative to the time of tornadogenesis, however, the trend in STP values is fairly flat. Interestingly, though, non-tornadic cases appear to show a declining trend immediately before and after peak mesocyclone intensity (Fig. 53). No clear trends are apparent in the sunset-relative STP values (Fig. 54). From Table 4, one can see that fixed STP did appear to have statistical

differences between tornadic and non-tornadic events with a two-sided p-value of 0.012, less than the threshold of 0.05 for statistical significance.

4.12 EBWD

With regards to Effective Bulk Wind Difference, there was an overall upward trend with the average values for both tornadic and non-tornadic cases (Fig. 55). Notably, there is significant overlap between the distributions as shown in Figure 56, indicating that EBWD is likely not to be a discriminatory parameter. Indeed, there is no discernable separation of tornadic and non-tornadic cases with respect to the time of tornadogenesis, peak mesocyclone intensity, or sunset (Figs. 57-58) which is consistent with the statistical analysis (Table 4) performed in which EBWD experienced a two-sided p-value of 0.1352, well above the 0.05 threshold for viewing statistical differences at the 5% study sample size seen in Table 3. From Table 4, one can see that EBWD did not appear to have statistical differences between tornadic and non-tornadic events with a two-sided p-value of 0.1352, greater than the threshold of 0.05 for statistical significance.

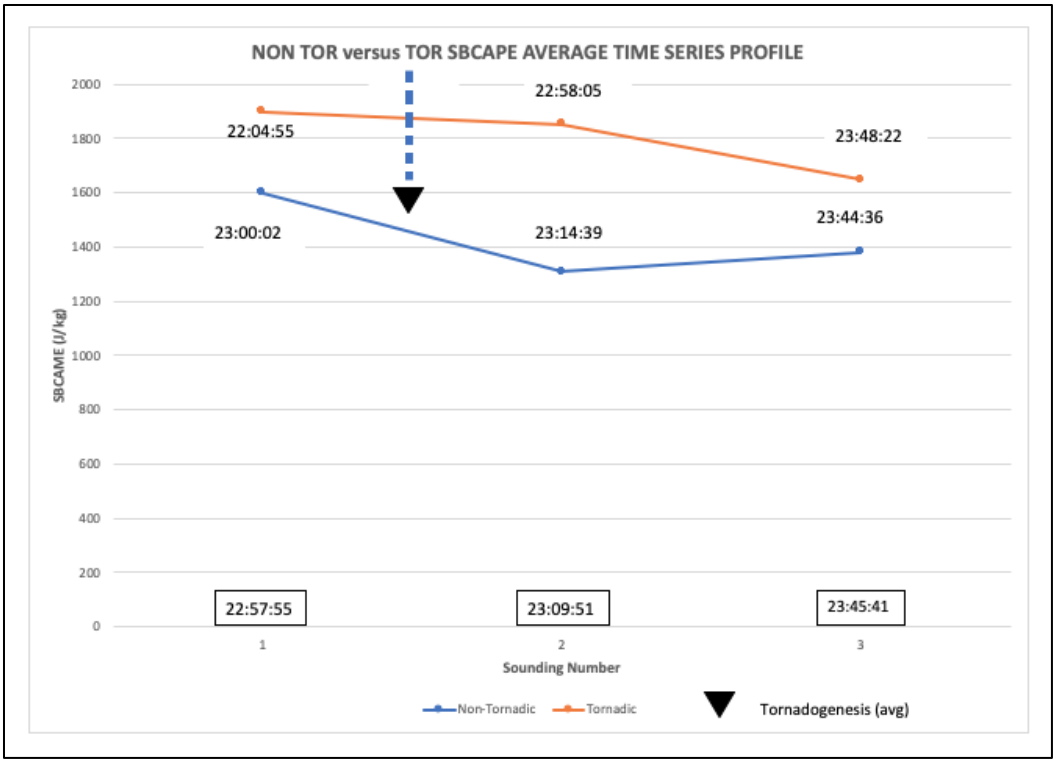

Figure 11. Non-tornadic versus tornadic surface based CAPE average time series profile through the first three inflow soundings of the 38 supercells observed. Average times of both events are attached to the respective lines while the overall average sounding times of the entire dataset is below just above the sounding number. Average time of tornadogenesis is present marked by a black 180 degree turned triangle.

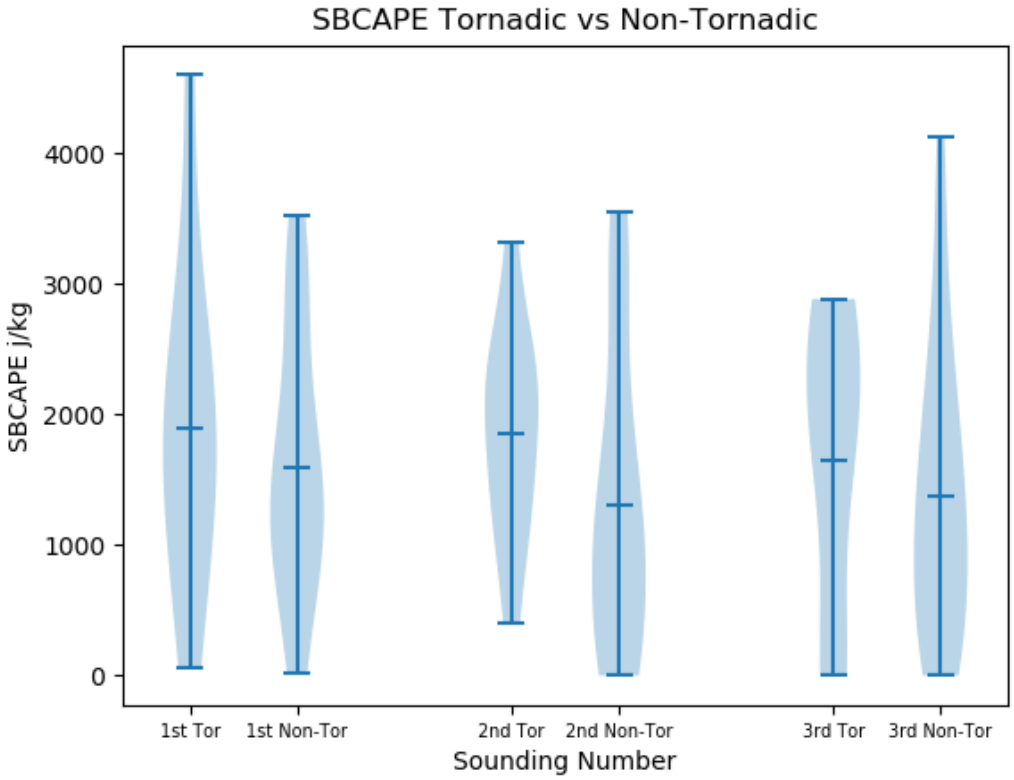

Figure 12. Violin distribution plot of SBCAPE for the tornadic and non-tornadic dataset with the middle line indicating the mean of each respective dataset. A wider appearing part of the violin type figure indicates where certain values are more common within the dataset.

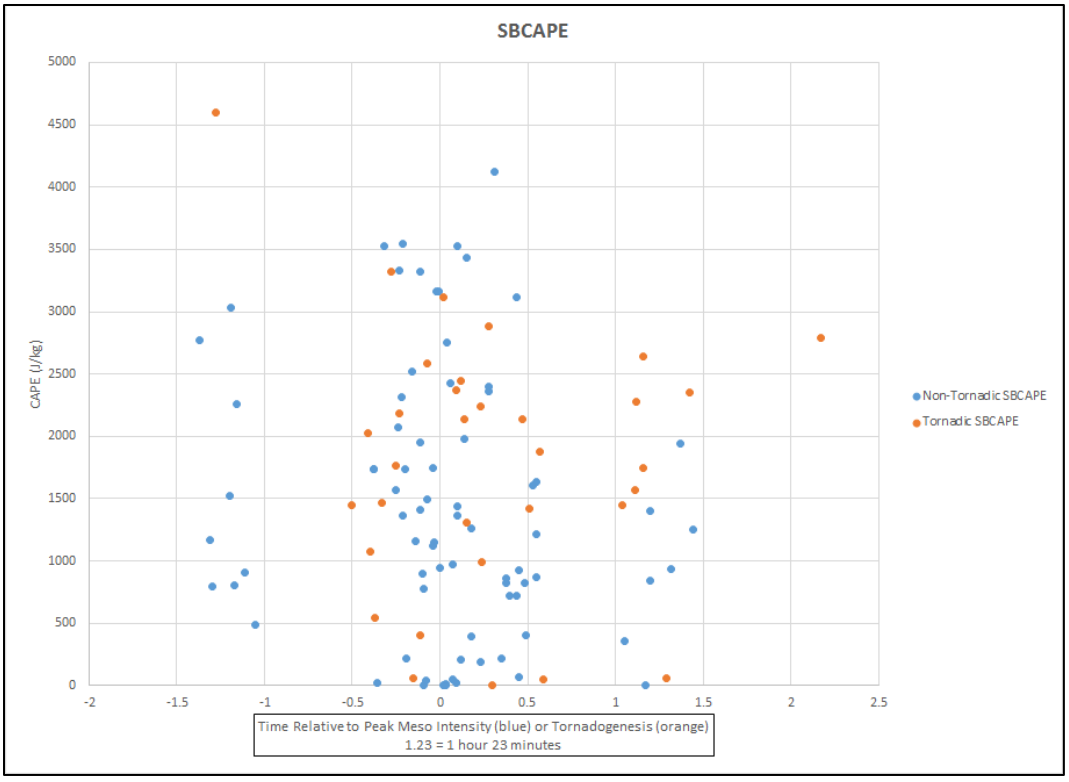

Figure 13. Distribution of SBCAPE values relative to time of peak mesocyclone intensity for non-tornadic cases (in blue) and tornadogenesis for tornadic cases (in orange).

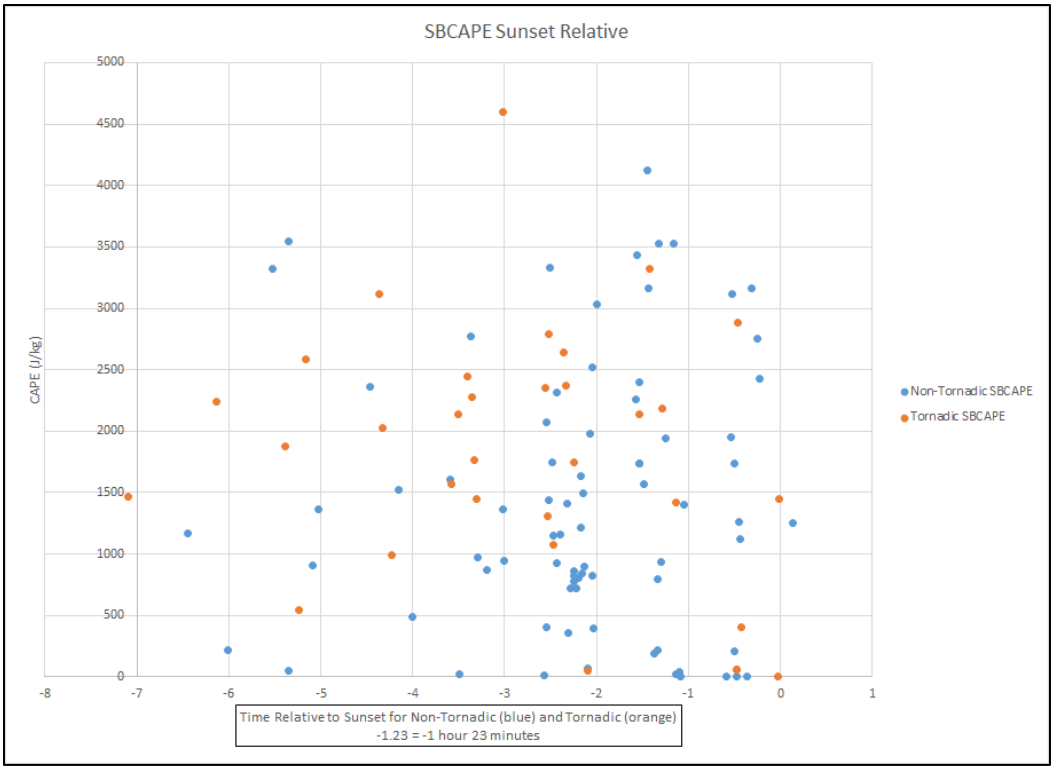

Figure 14. Distribution of SBCAPE values relative to time of sunset for non-tornadic cases (in blue) and tornadic cases (in orange).

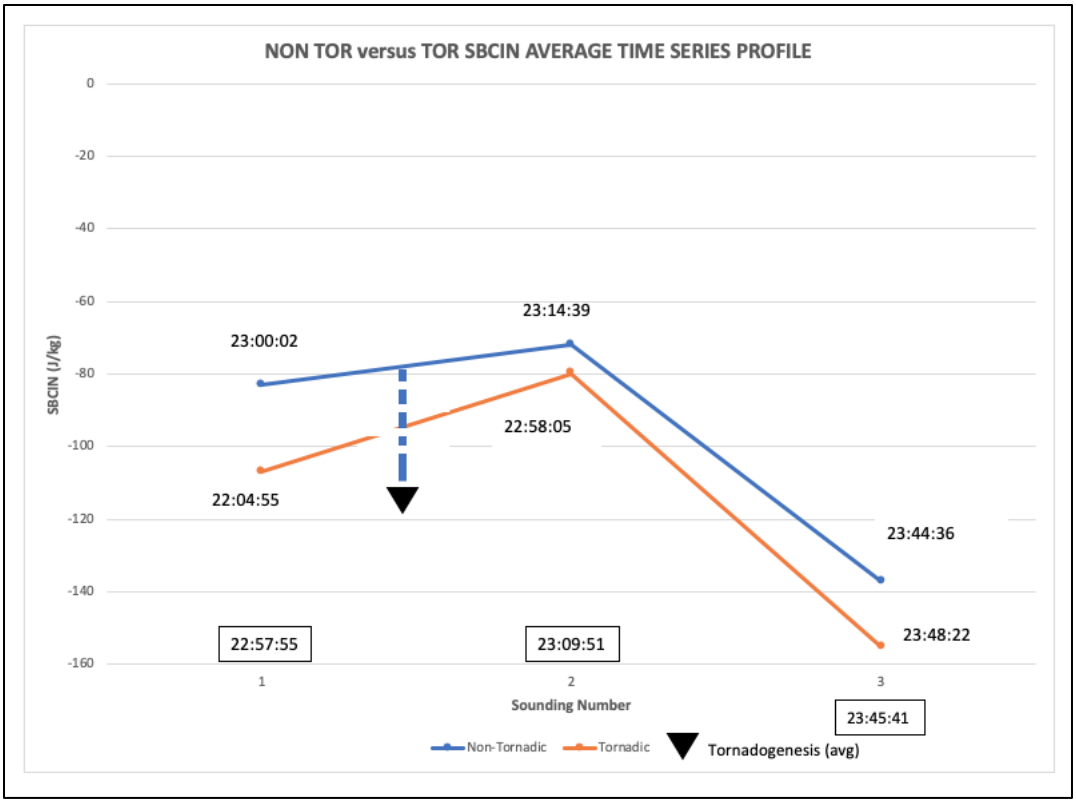

Figure 15. As in Fig. 11, but for SBCIN values.

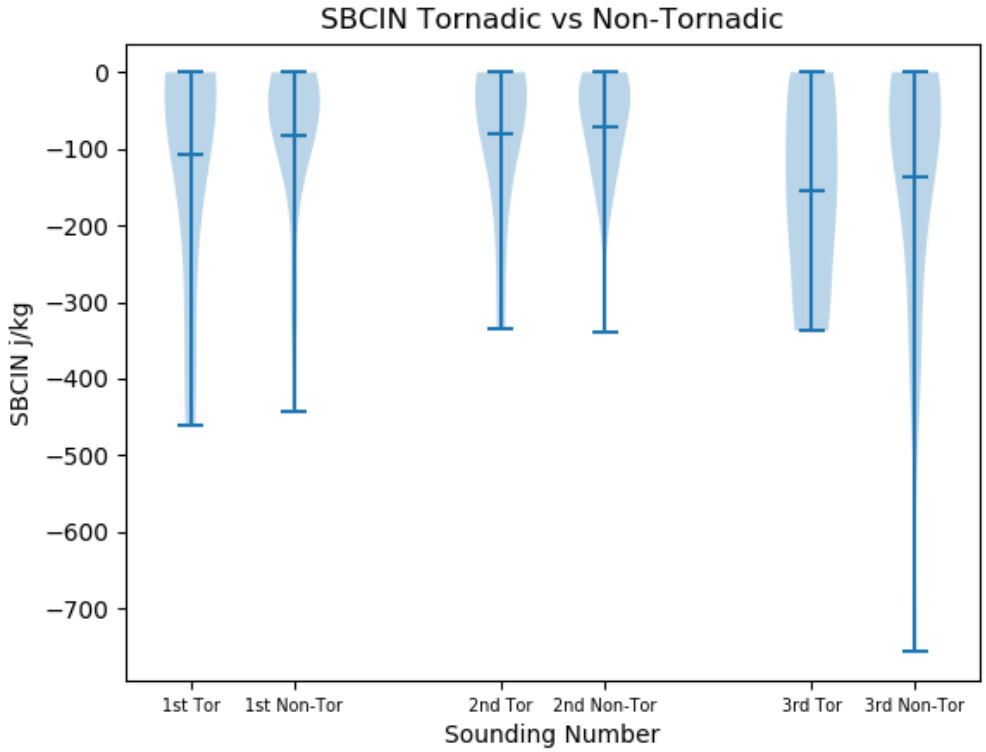

Figure 16. As in Fig. 12, but for SBCIN values.

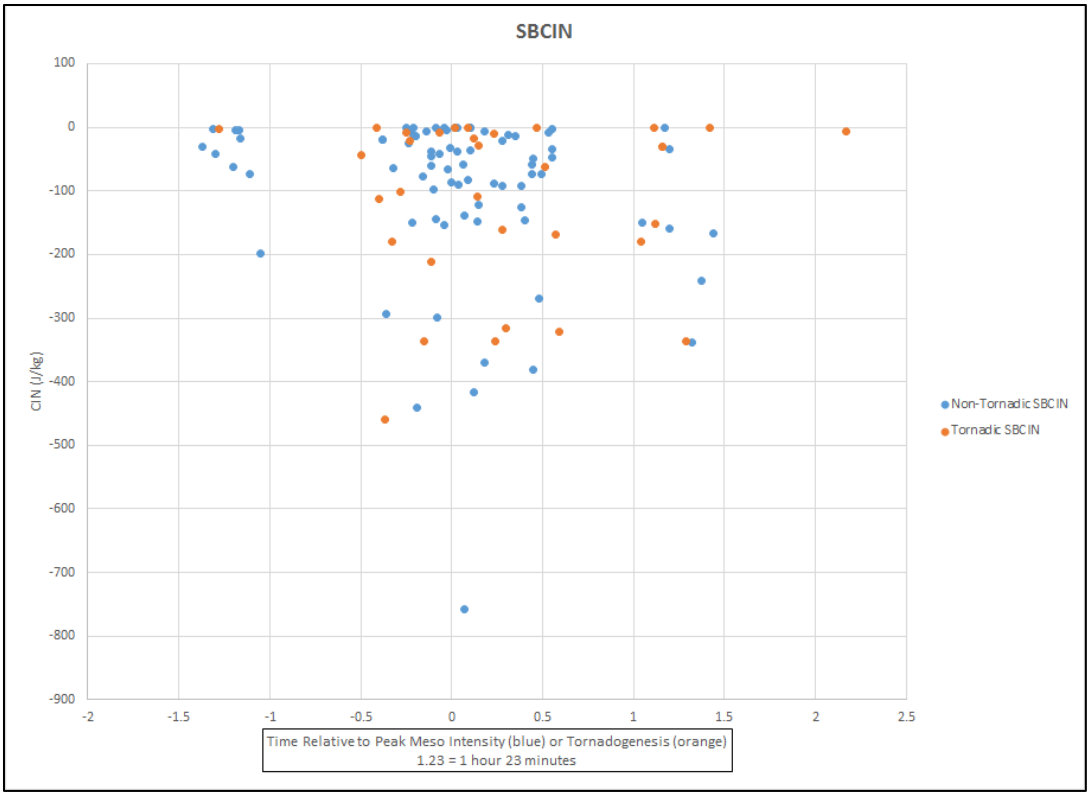

Figure 17. As in Fig. 13, but for SBCIN values.

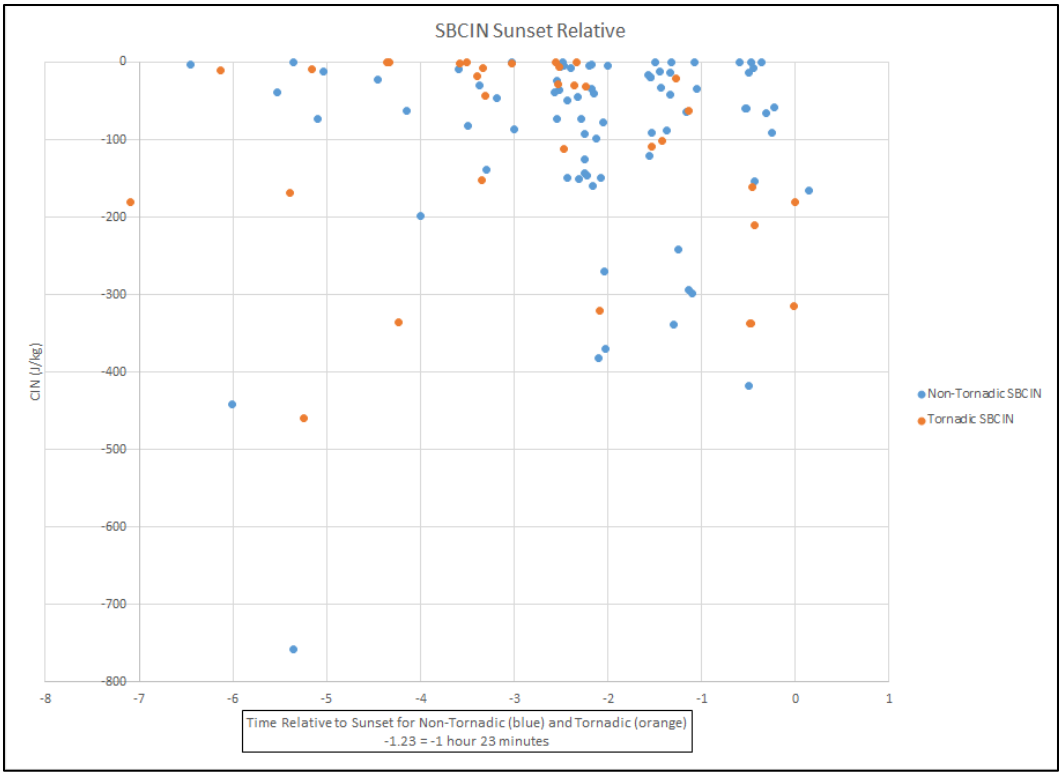

Figure 18. As in Fig. 14, but for SBCIN values.

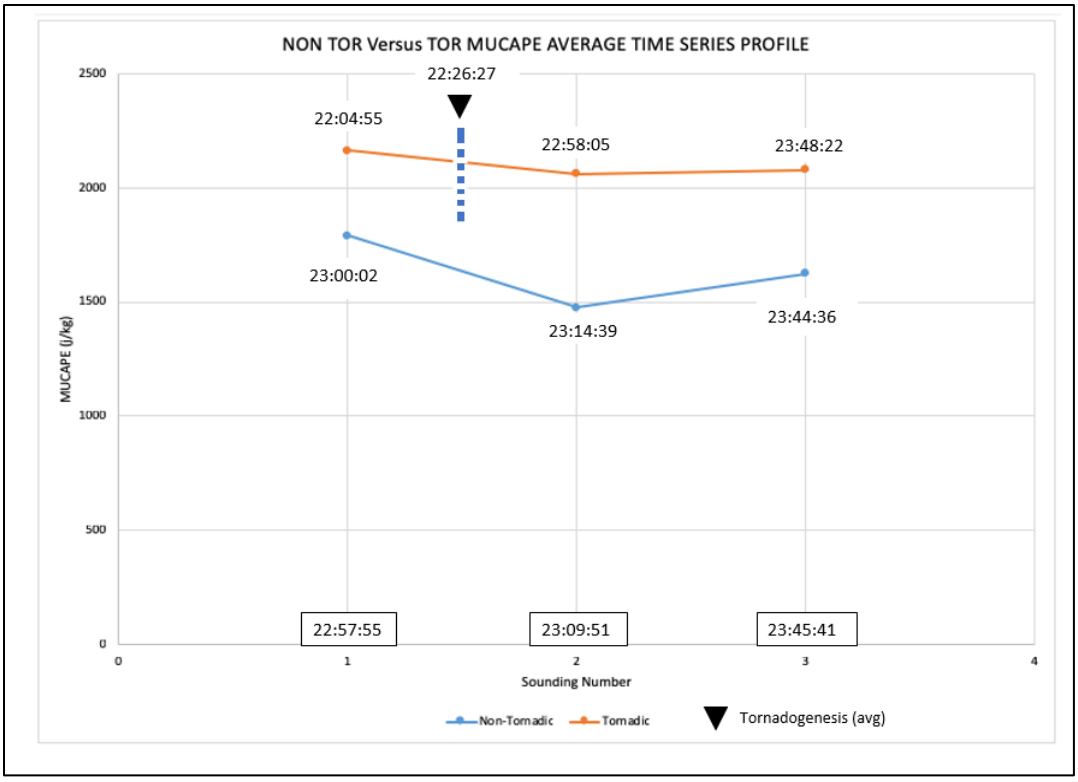

Figure 19. As in Fig. 11, but for MUCAPE values.

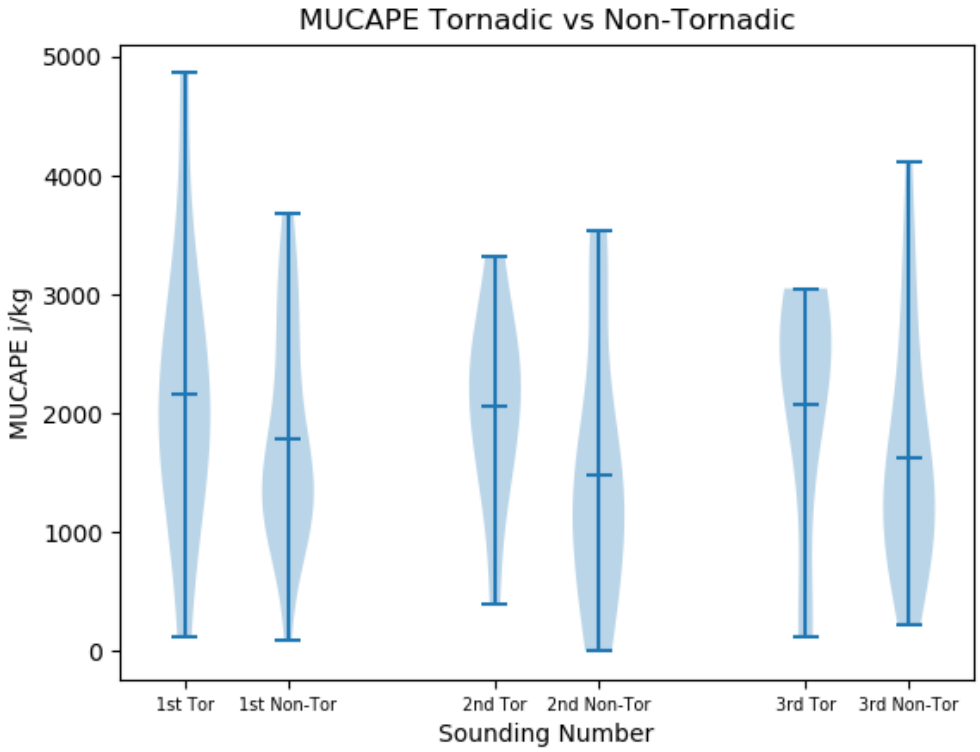

Figure 20. As in Fig. 12, but for MUCAPE values.

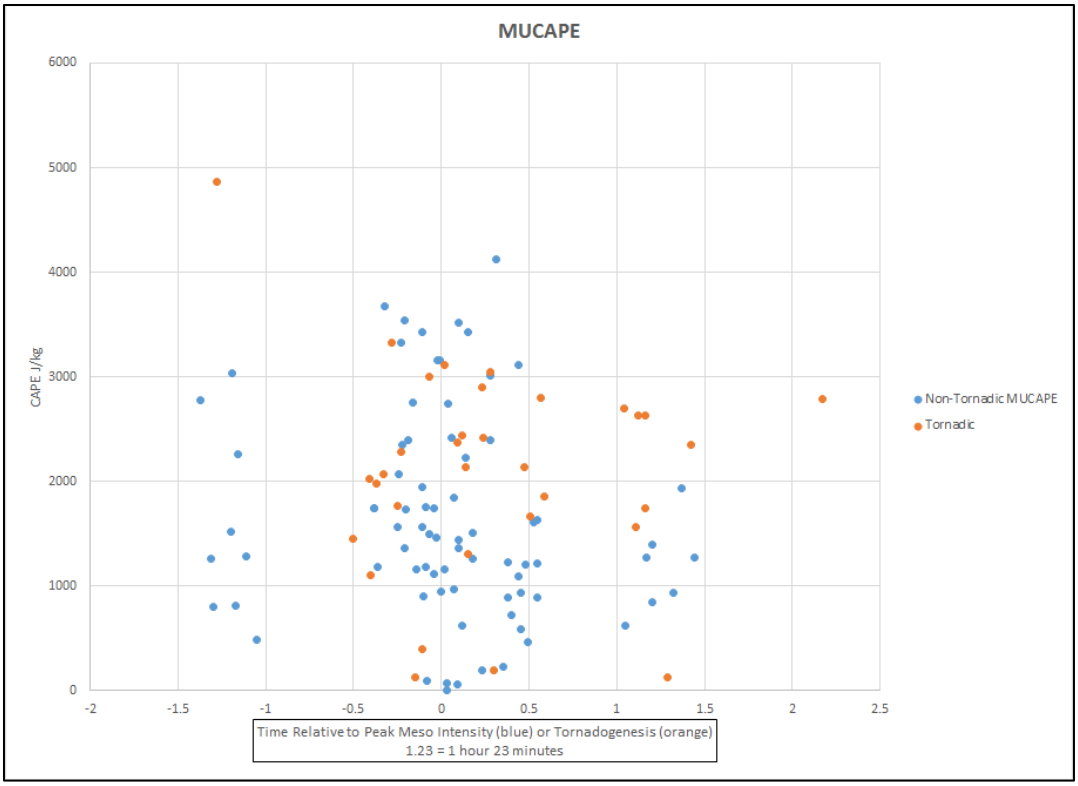

Figure 21. As in Fig. 13, but for MUCAPE values.

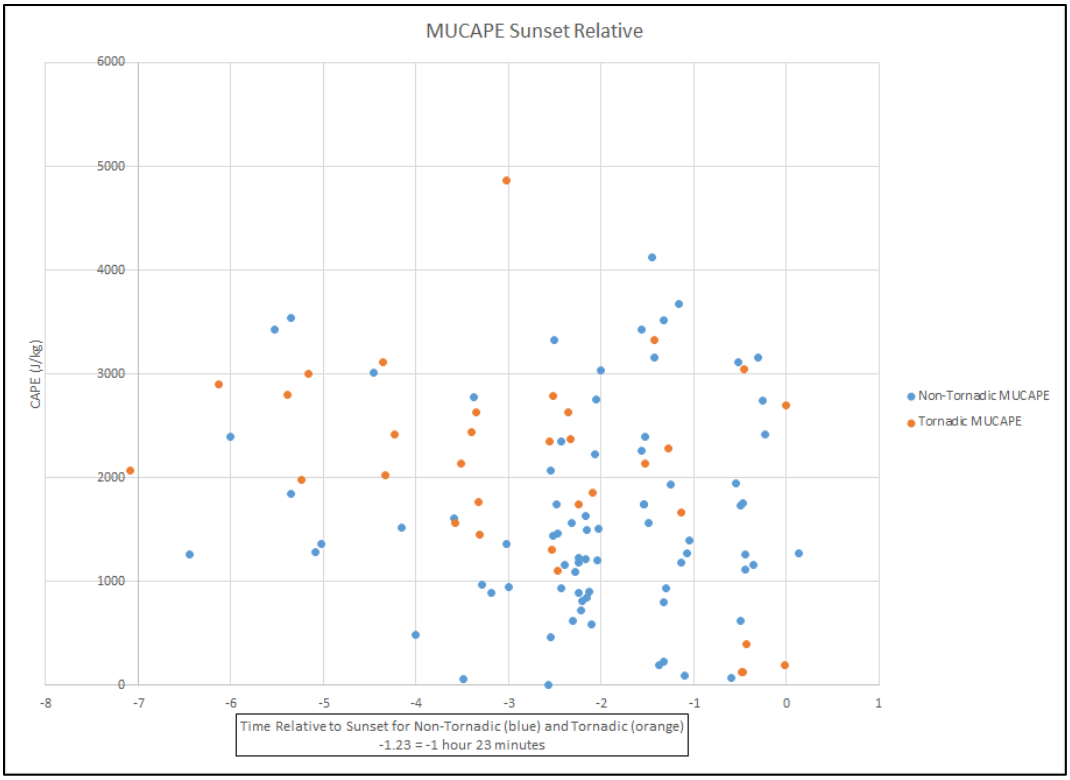

Figure 22. As in Fig.14, but for MUCAPE values.

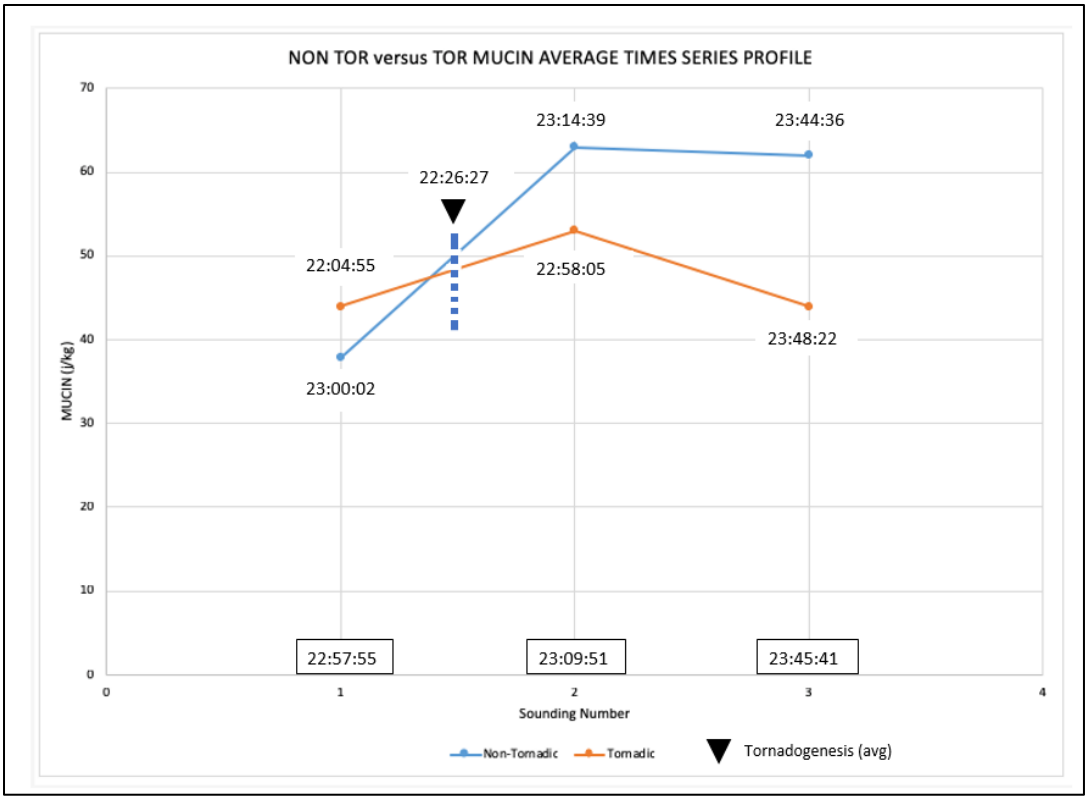

Figure 23. As in Fig. 11, but for MUCIN values.

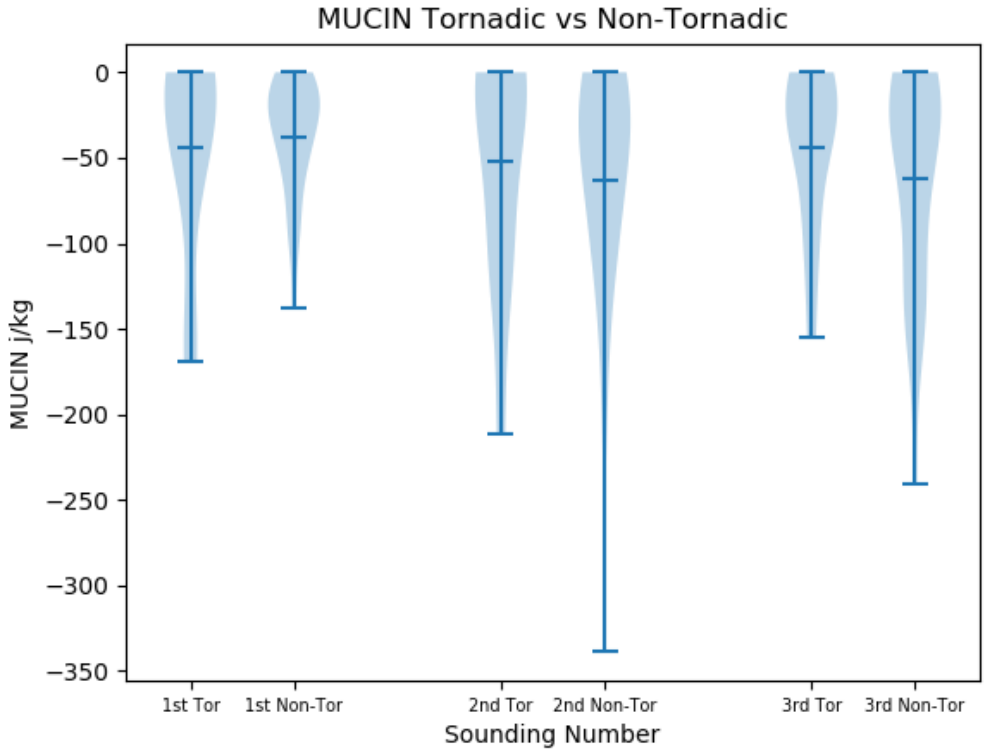

Figure 24. As in Fig. 12, but for MUCIN values.

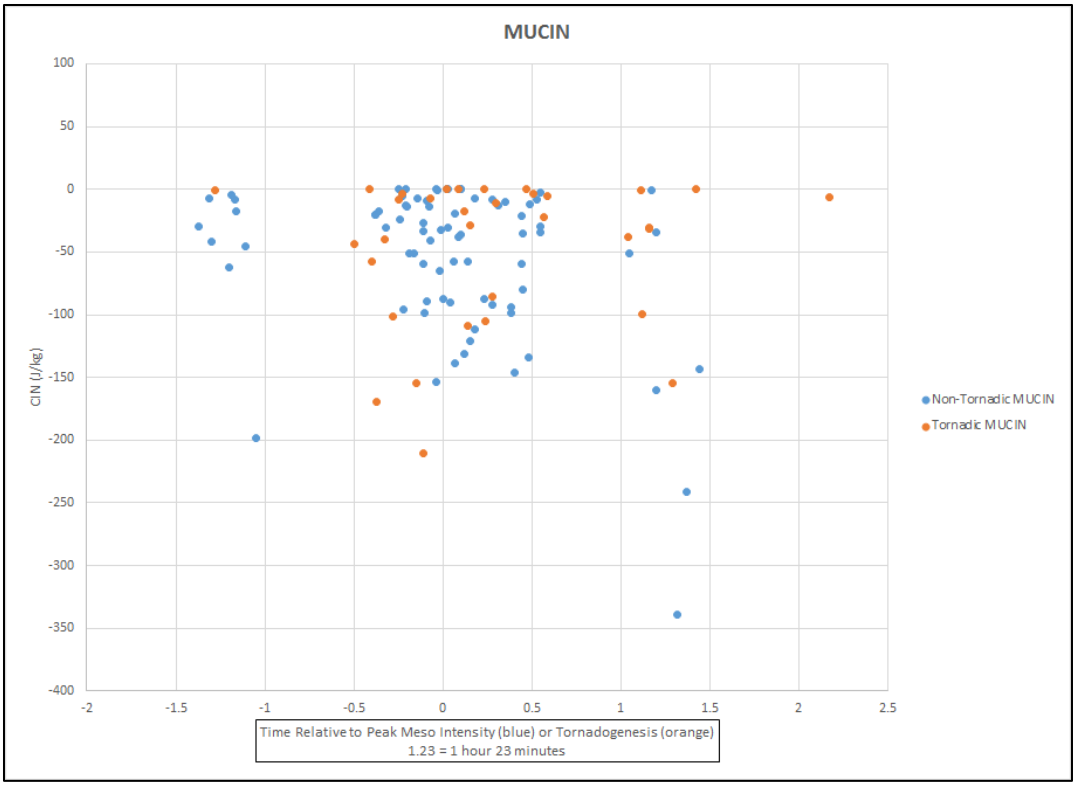

Figure 25. As in Fig. 13, but for MUCIN values.

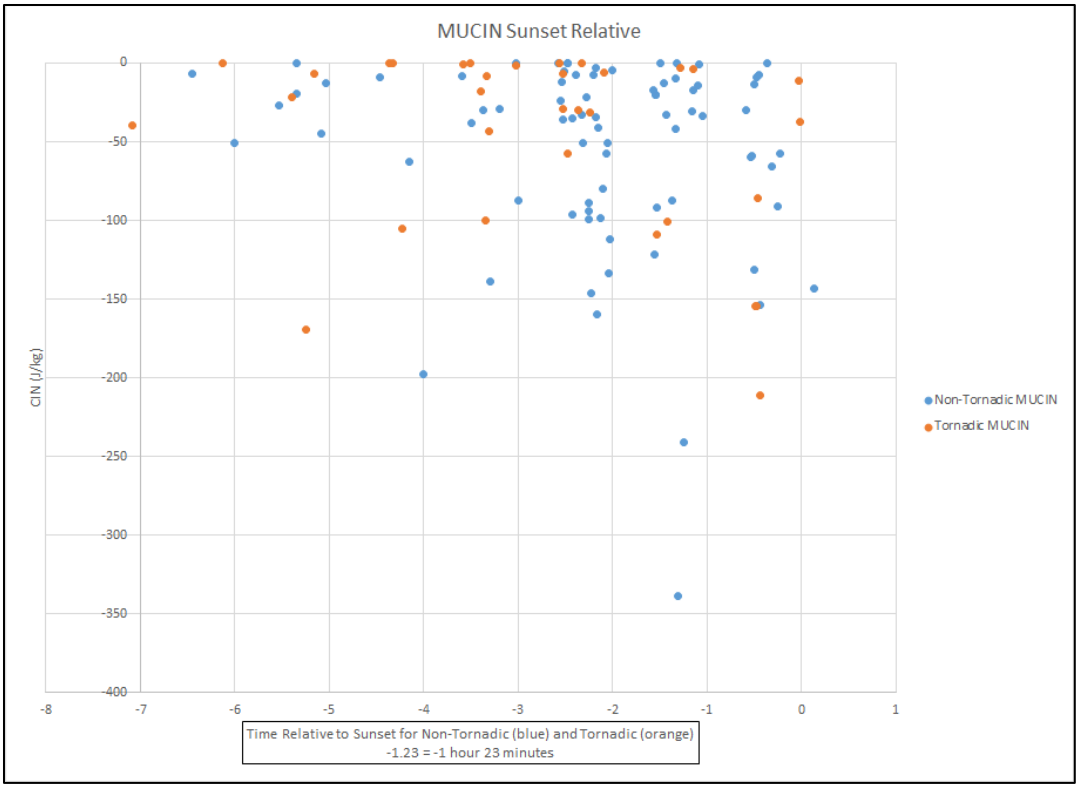

Figure 26. As in Fig. 14, but for MUCIN values.

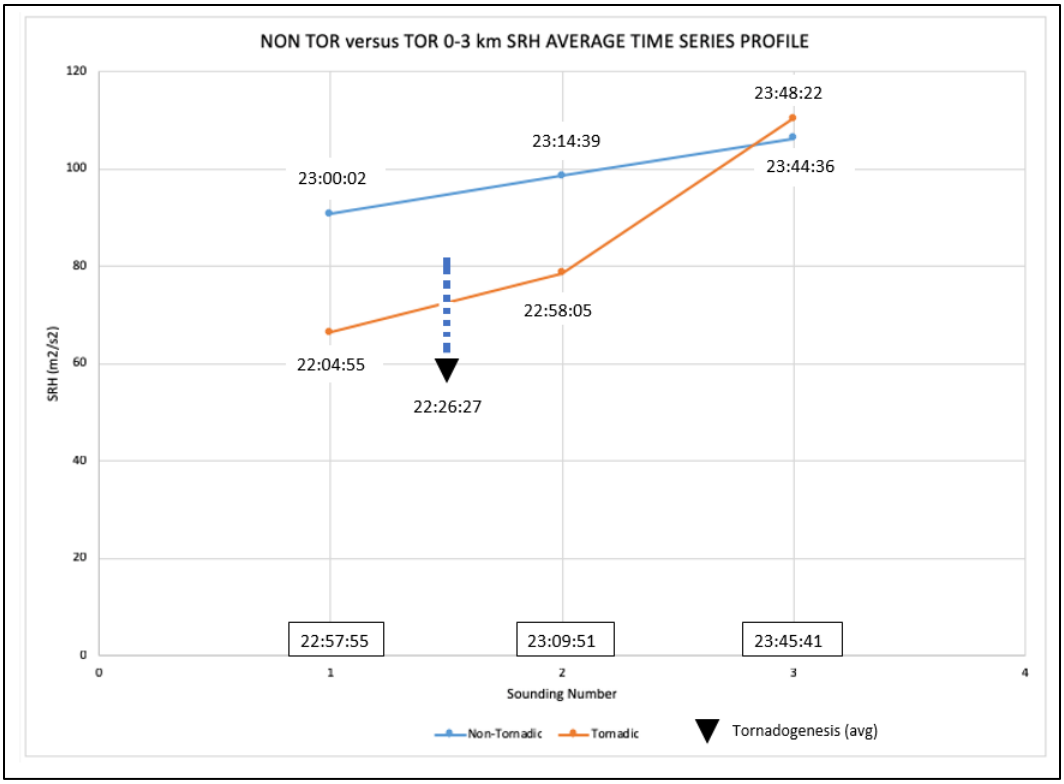

Figure 27. As in Fig. 11, but for 0 to 3 km SRH values.

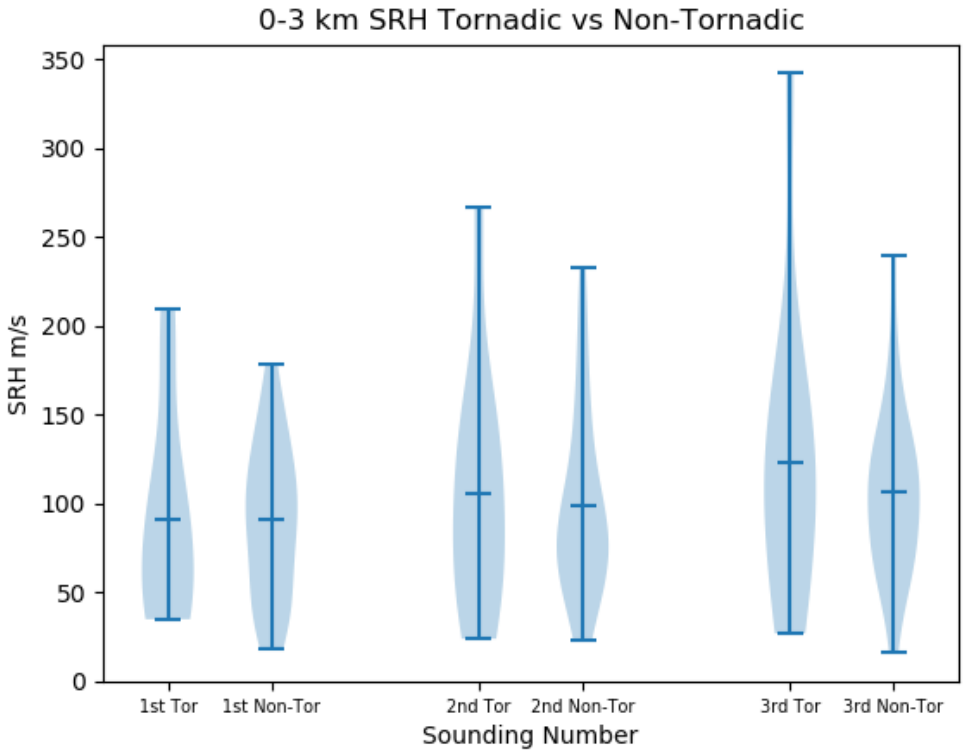

Figure 28. As in Fig. 12, but for 0 to 3 km SRH values.

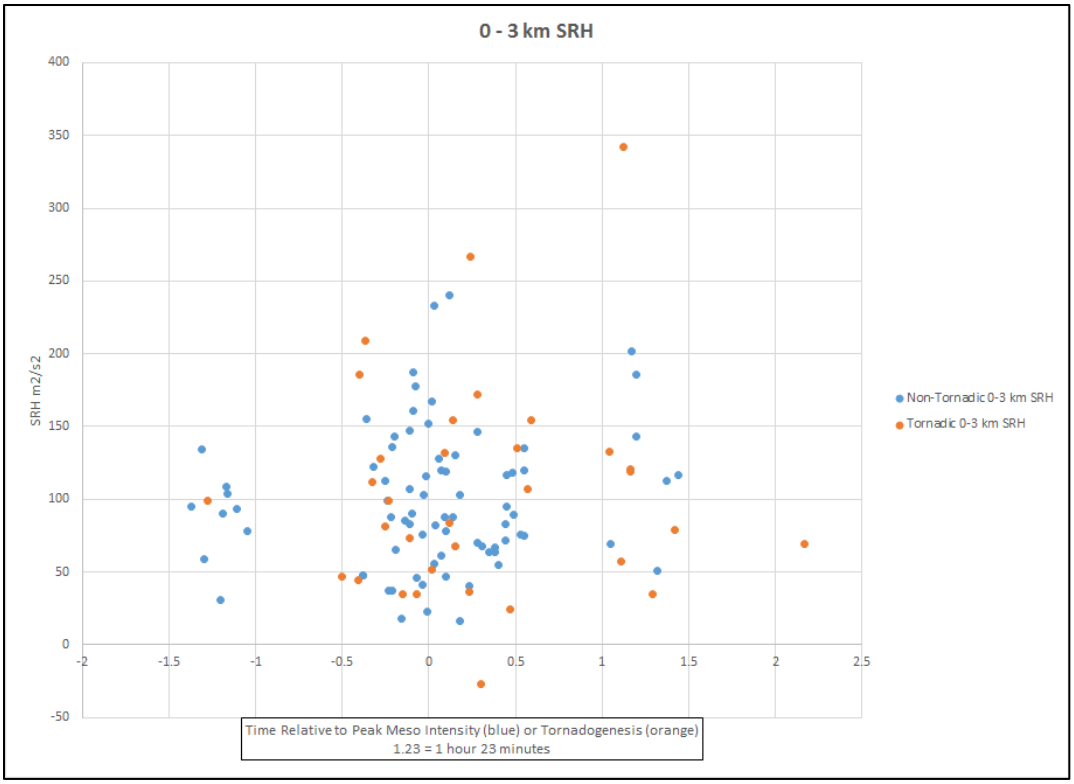

Figure 29. As in Fig. 13, but for 0 to 3 km SRH values.

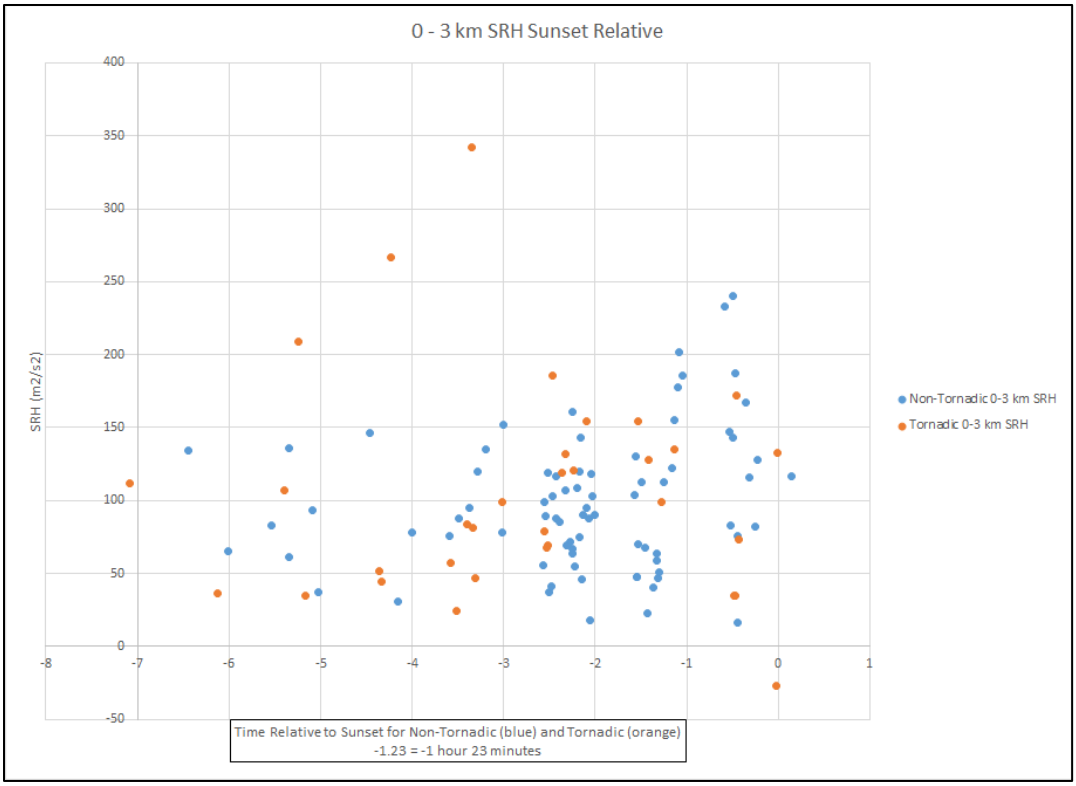

Figure 30. As in Fig. 14, but for 0 to 3 km SRH values.

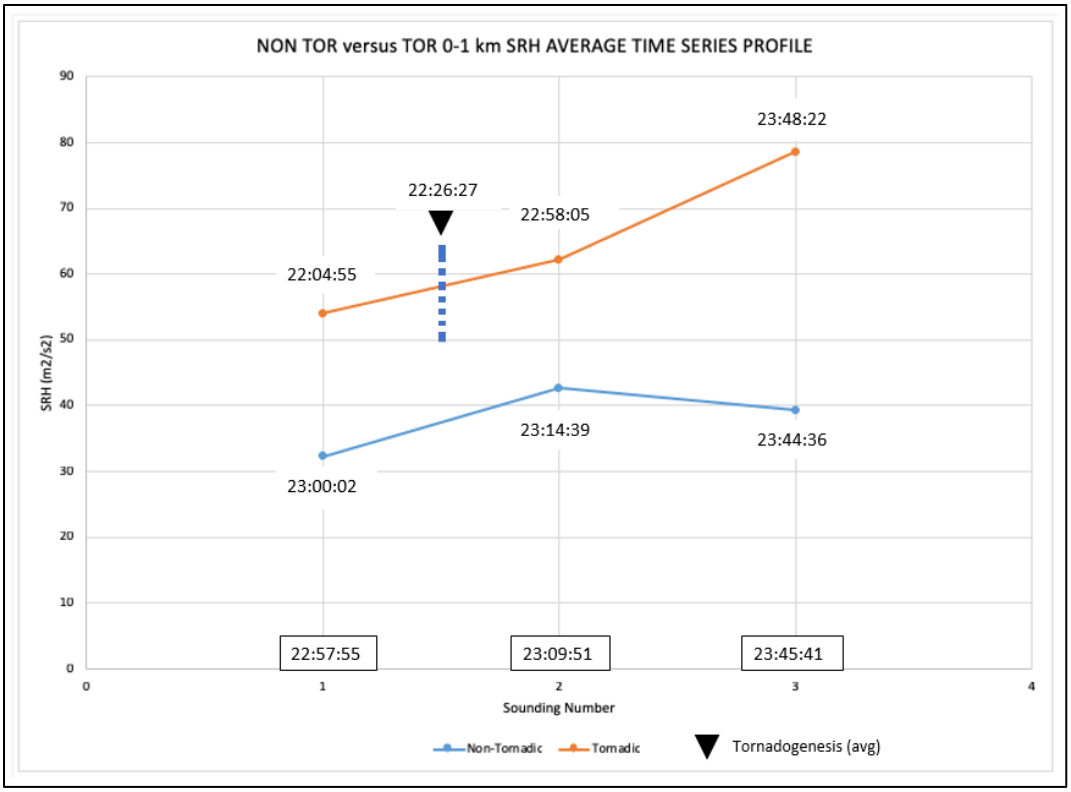

Figure 31. As in Fig. 11, but for 0 to 1 km SRH values.

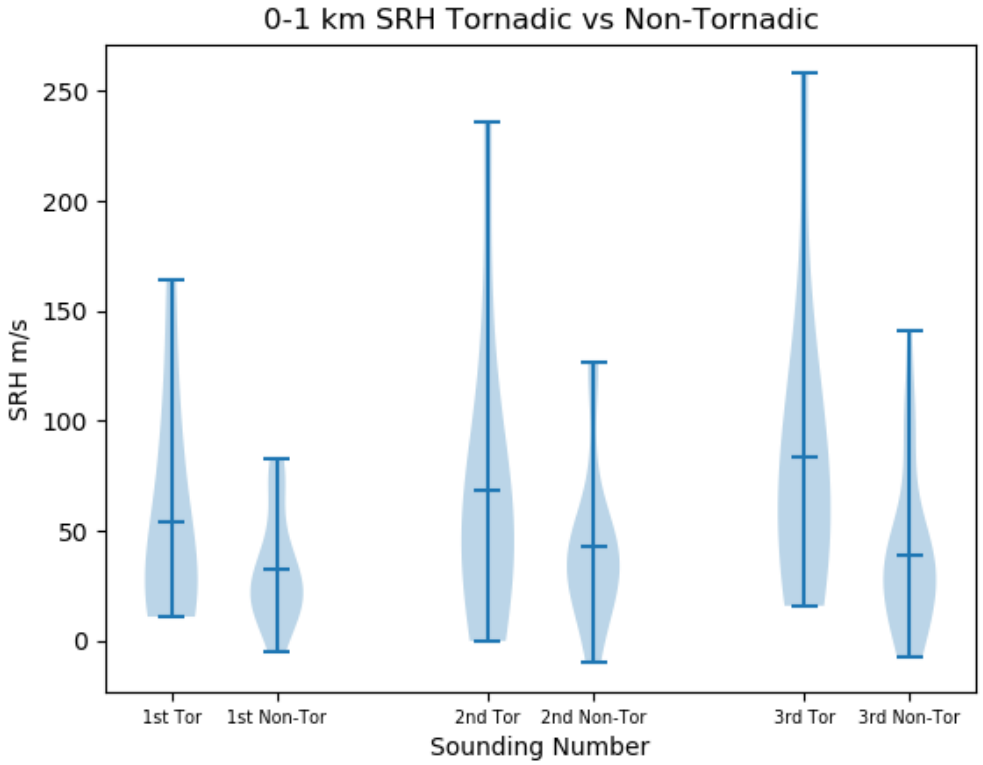

Figure 32. As in Fig. 12, but for 0 to 1 km SRH values.

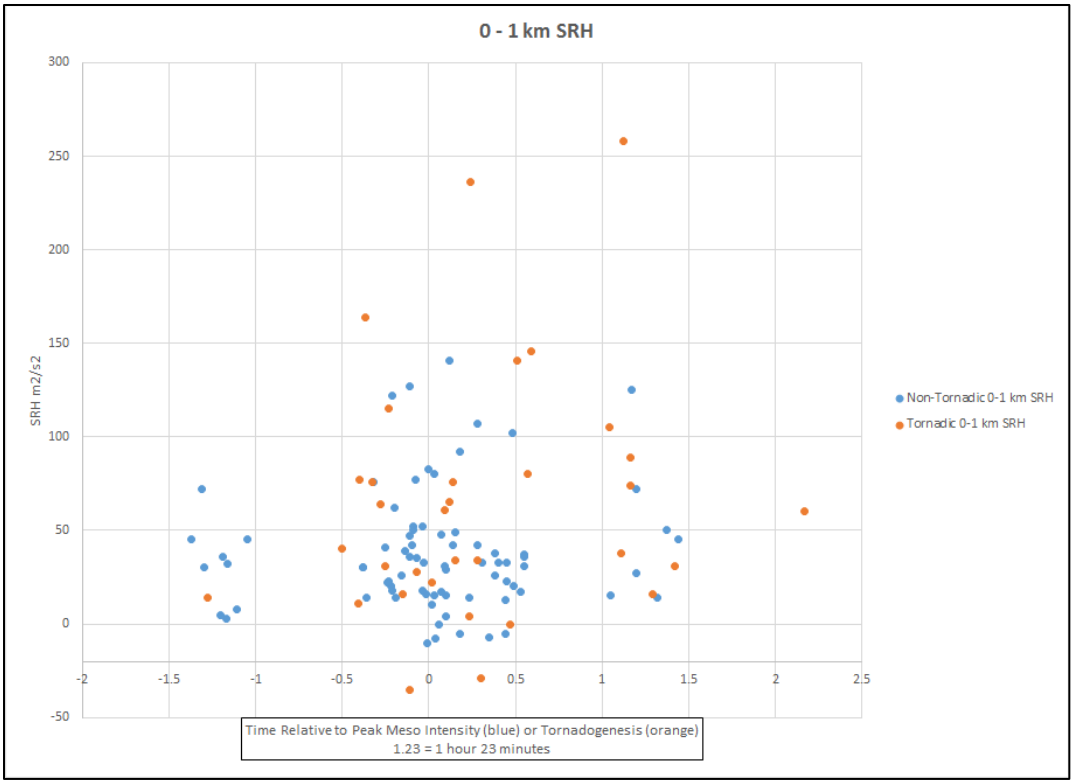

Figure 33. As in Fig. 13, but for 0 to 1 km SRH values.

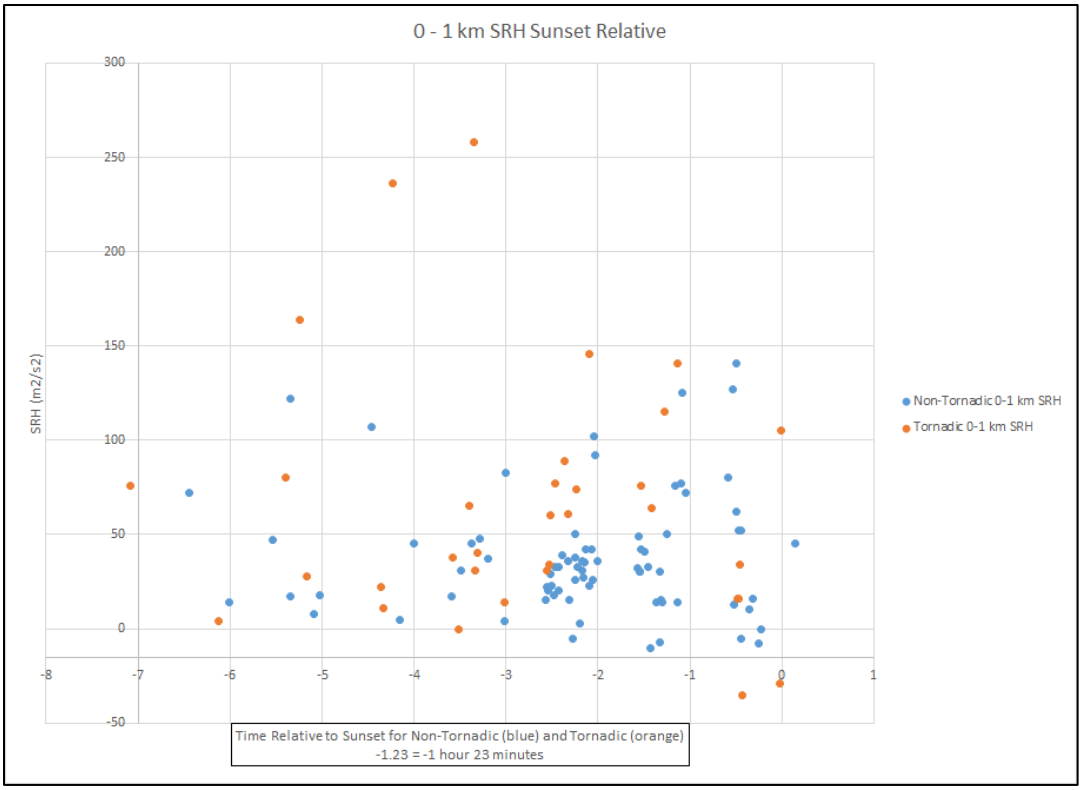

Figure 34. As in Fig. 14, but for 0 to 1 km SRH values.

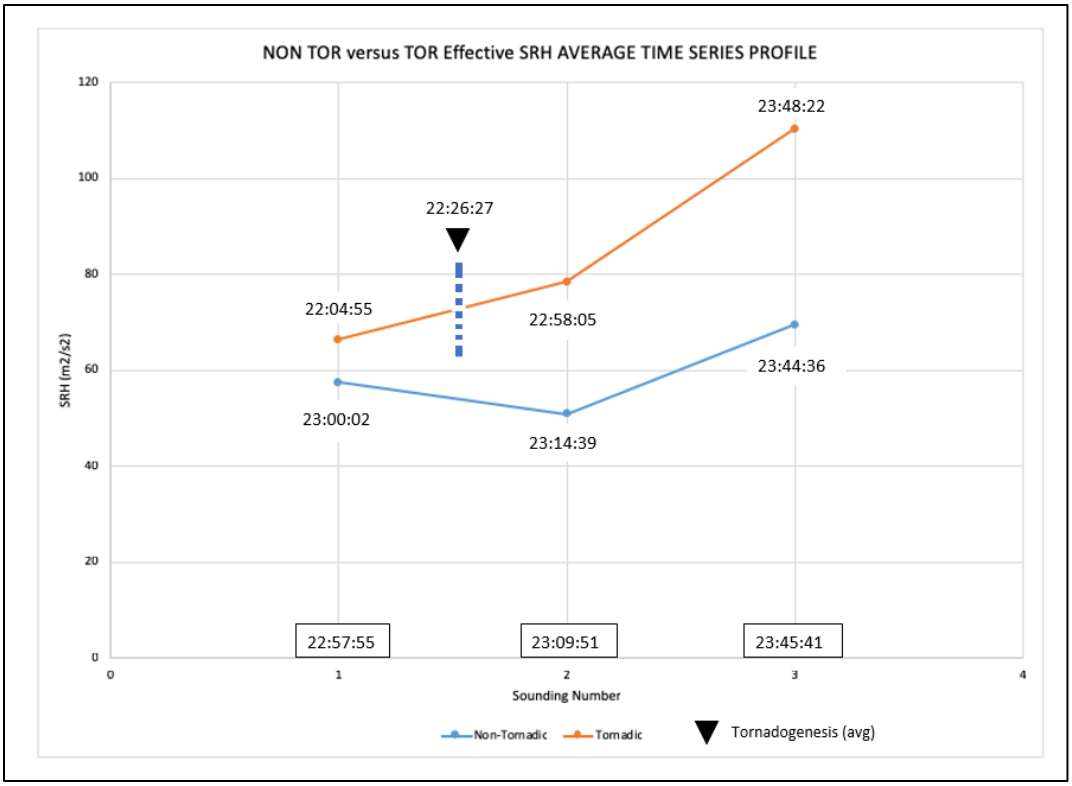

Figure 35. As in Fig. 11, but for Effective SRH values.

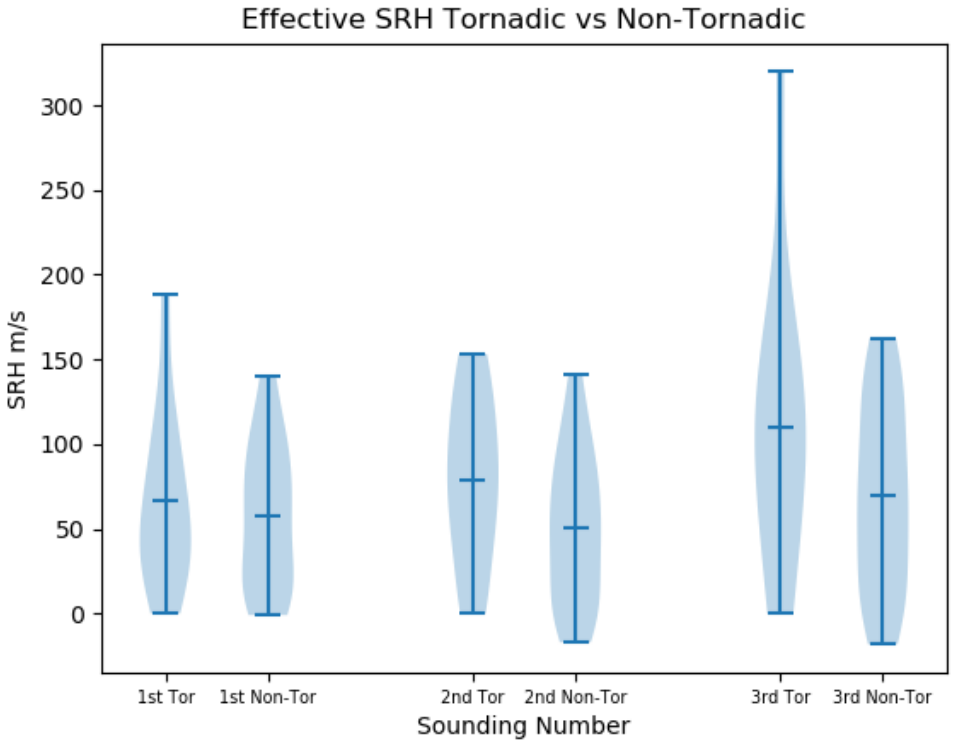

Figure 36. As in Fig. 12, but for Effective SRH values.

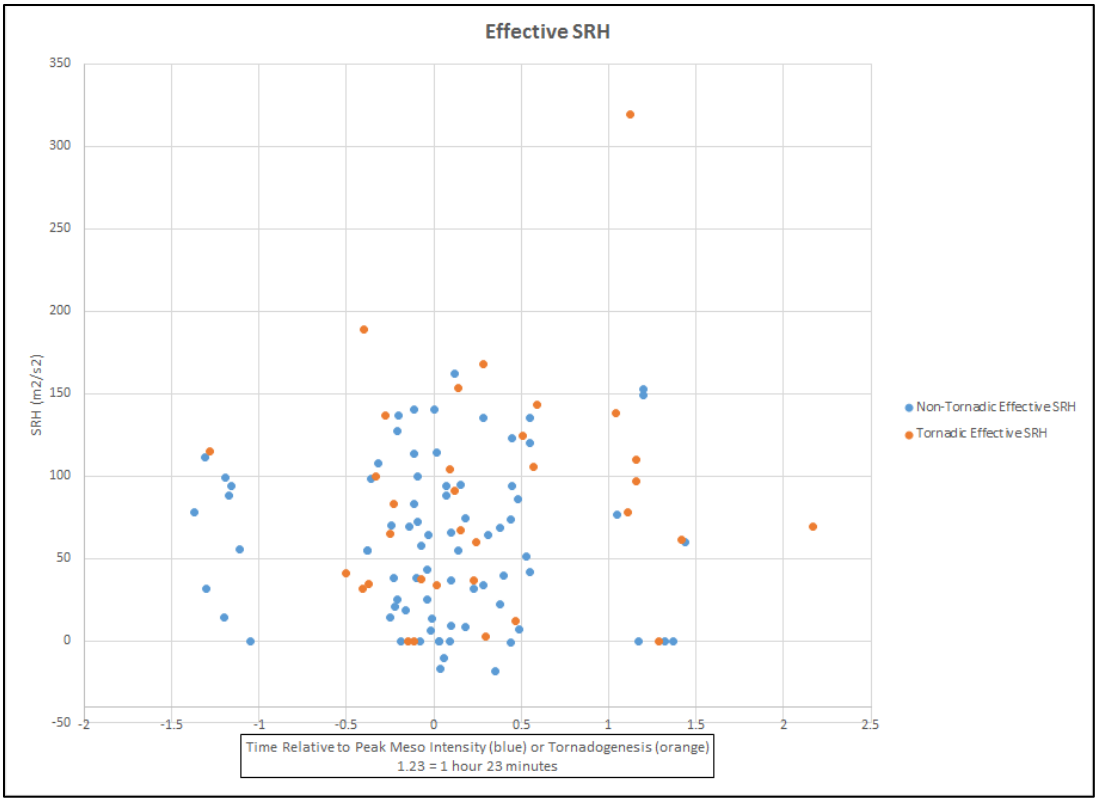

Figure 37. As in Fig. 13, but for Effective SRH values.

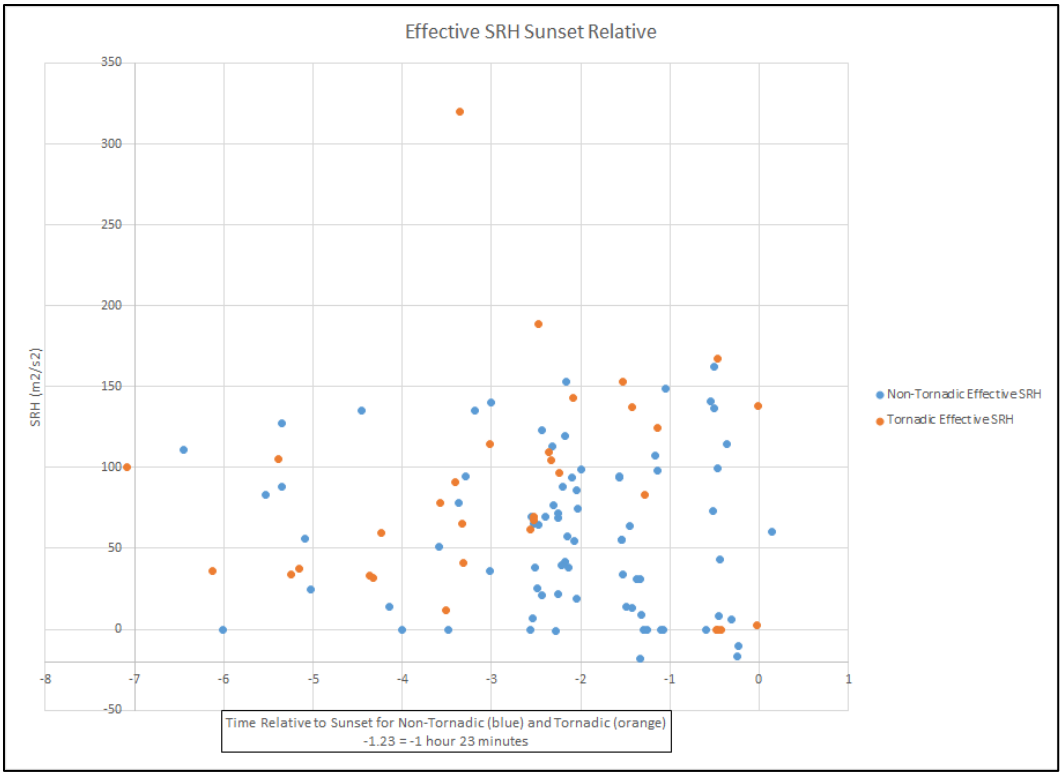

Figure 38. As in Fig. 14, but for Effective SRH values.

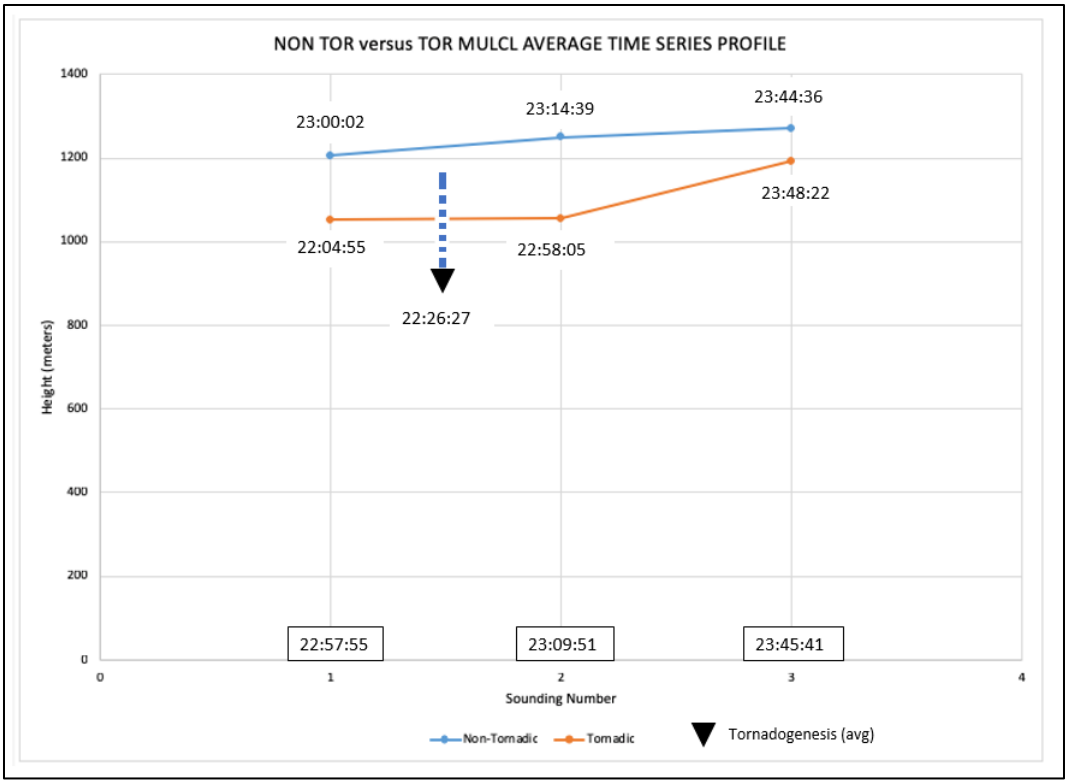

Figure 39. As in Fig. 11, but for MULCL values.

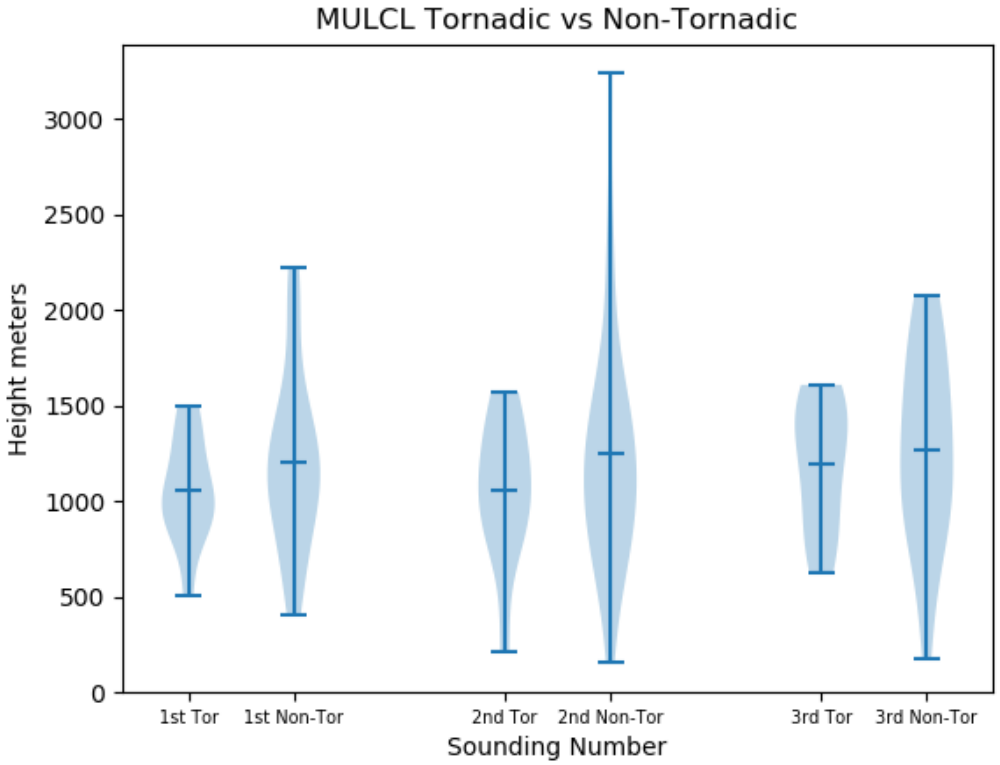

Figure 40. As in Fig. 12, but for MULCL values.

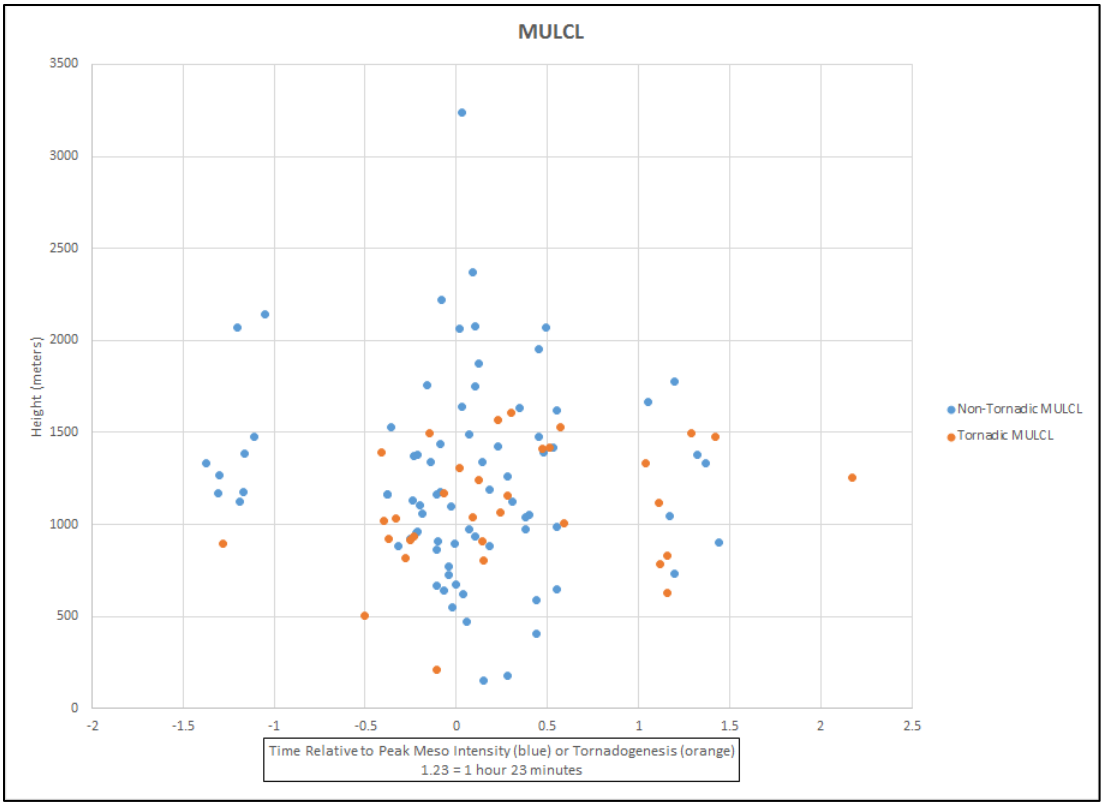

Figure 41. As in Fig. 13, but for MULCL values.

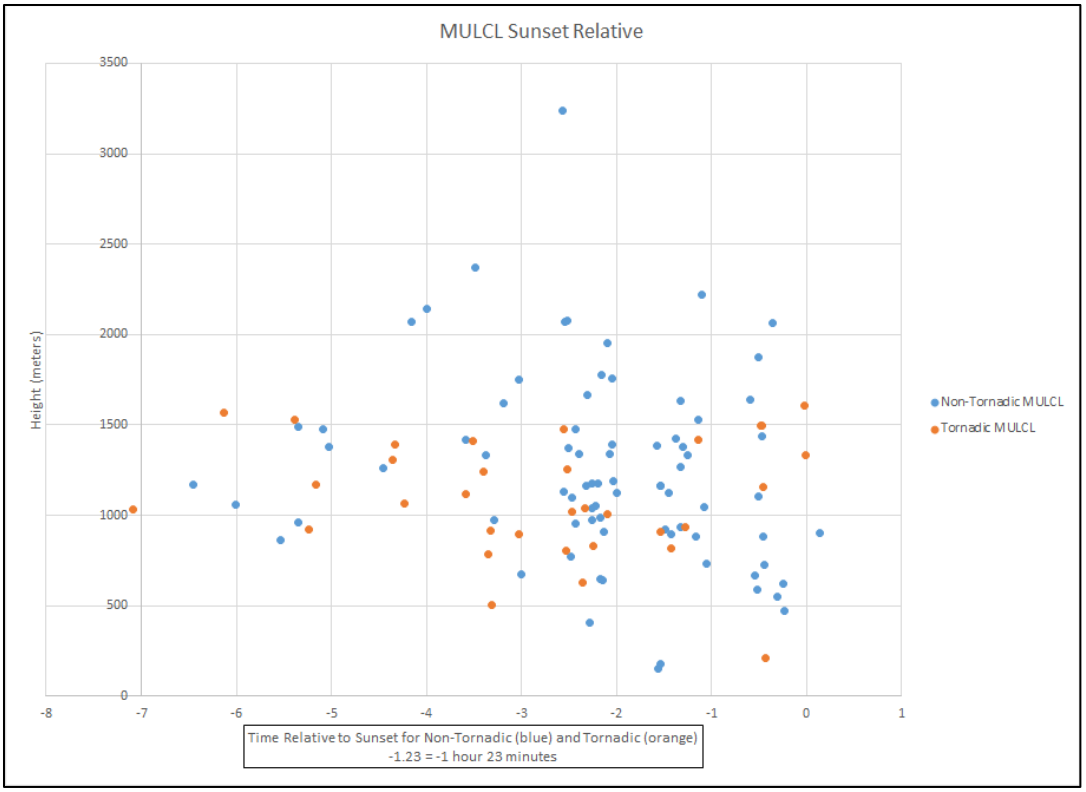

Figure 42. As in Fig. 14, but for MULCL values.

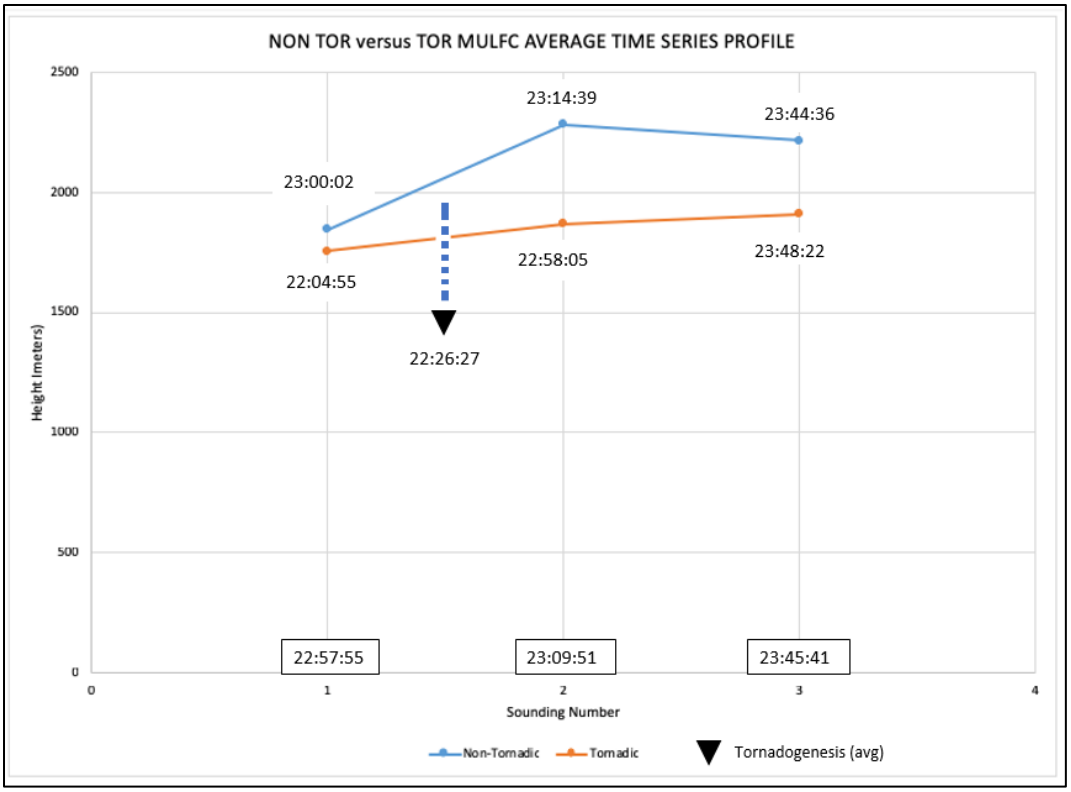

Figure 43. As in Fig. 11, but for MULFC values.

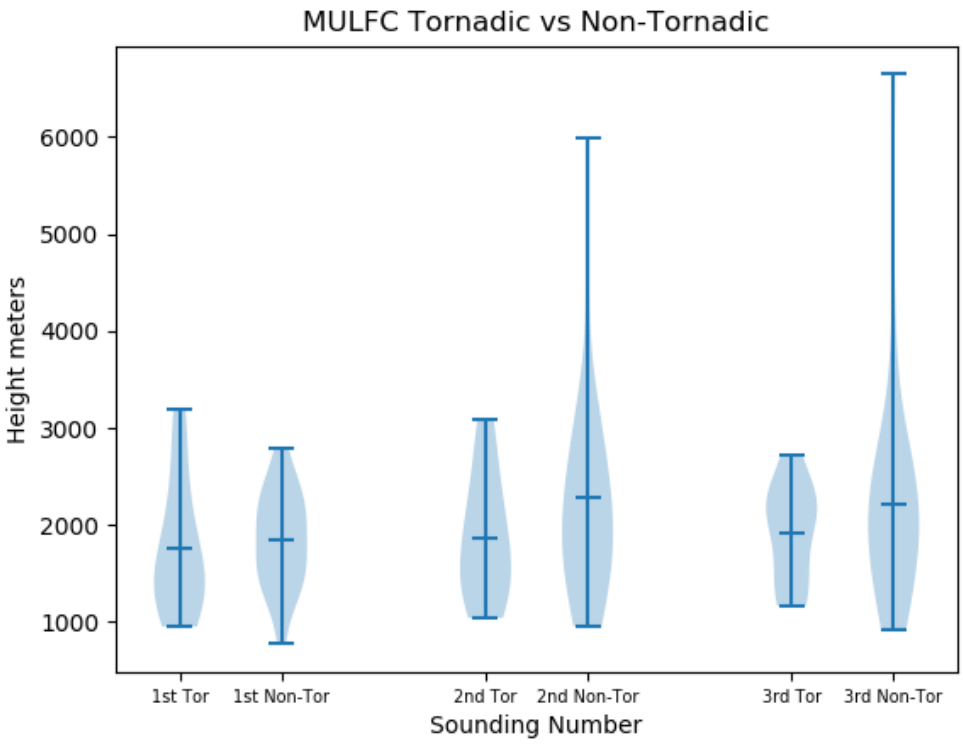

Figure 44. As in Fig. 12, but for MULFC values.

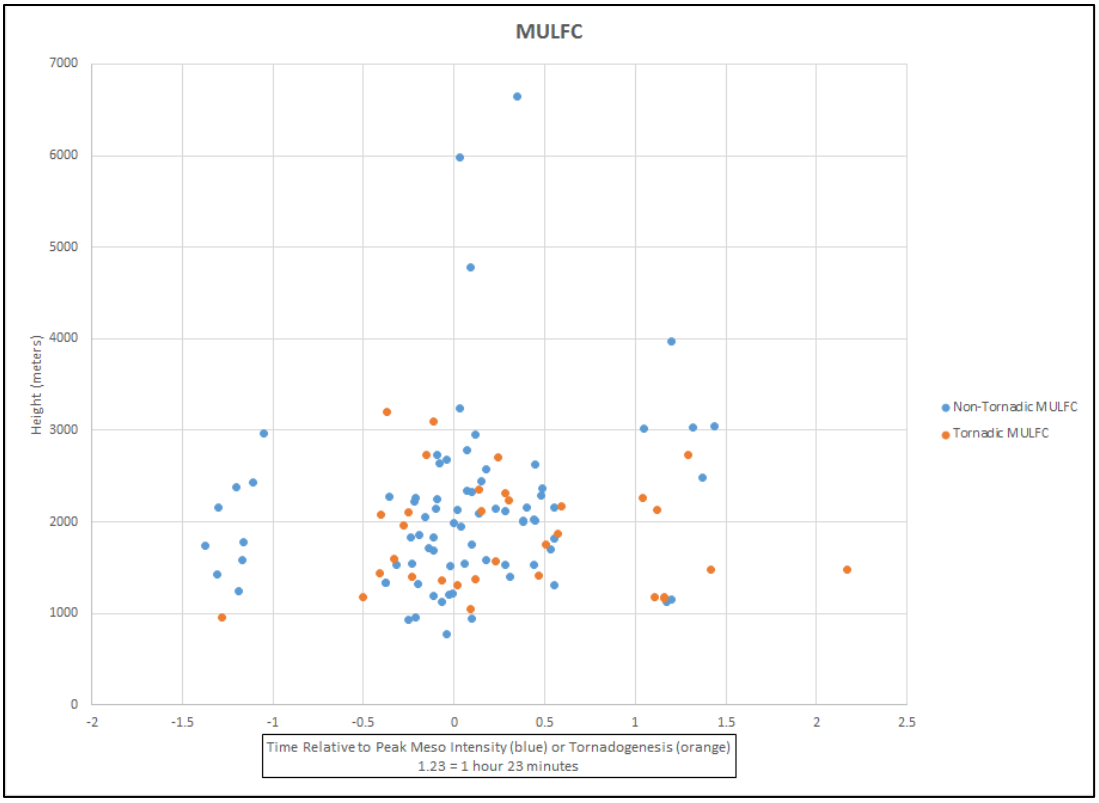

Figure 45. As in Fig. 13, but for MULFC values.

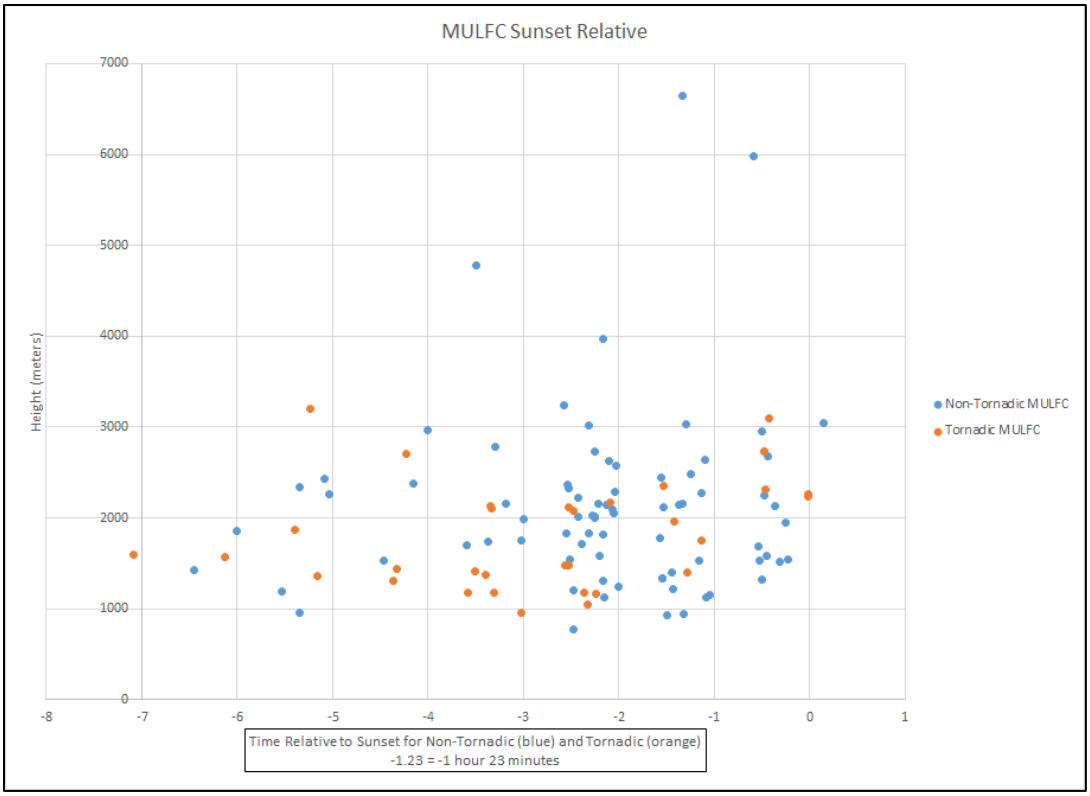

Figure 46. As in Fig. 14, but for MULFC values.

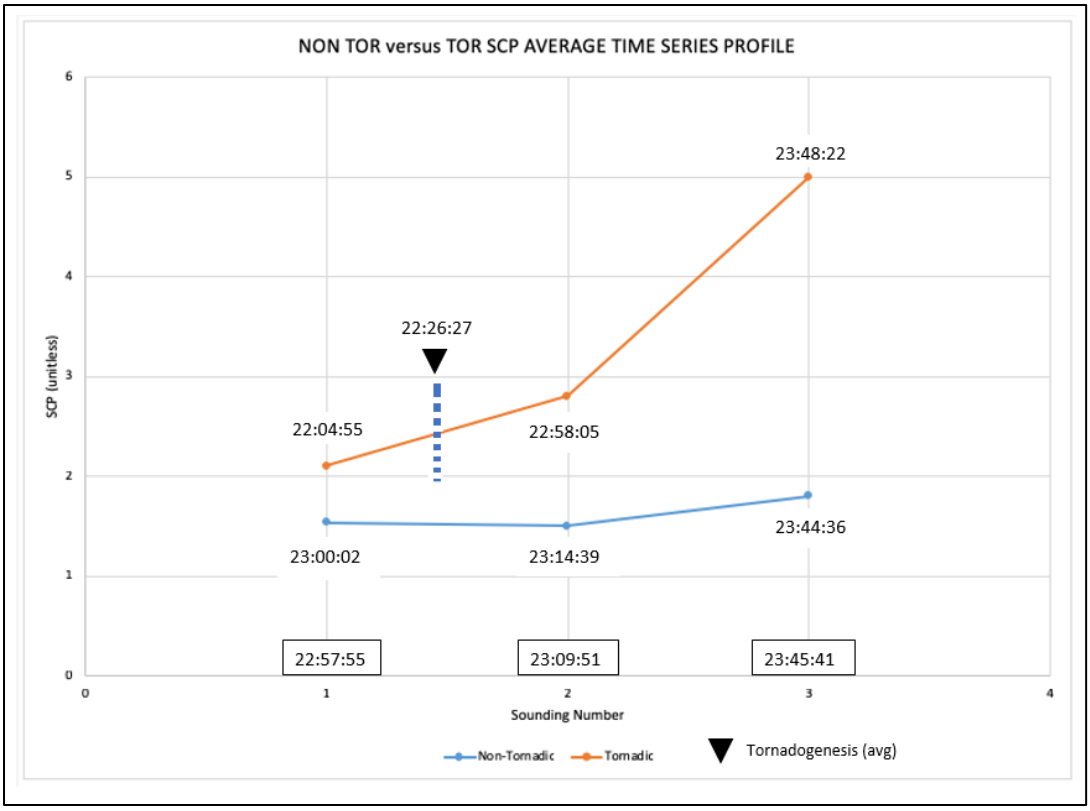

Figure 47. As in Fig. 11, but for SCP values.

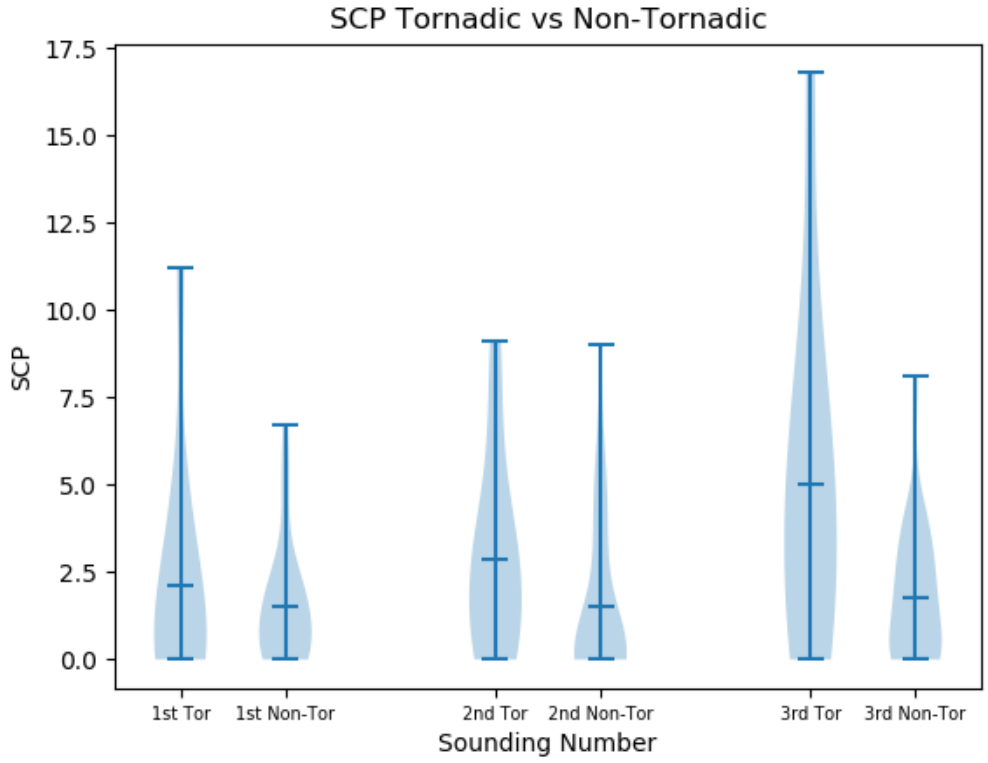

Figure 48. As in Fig. 12, but for SCP values.

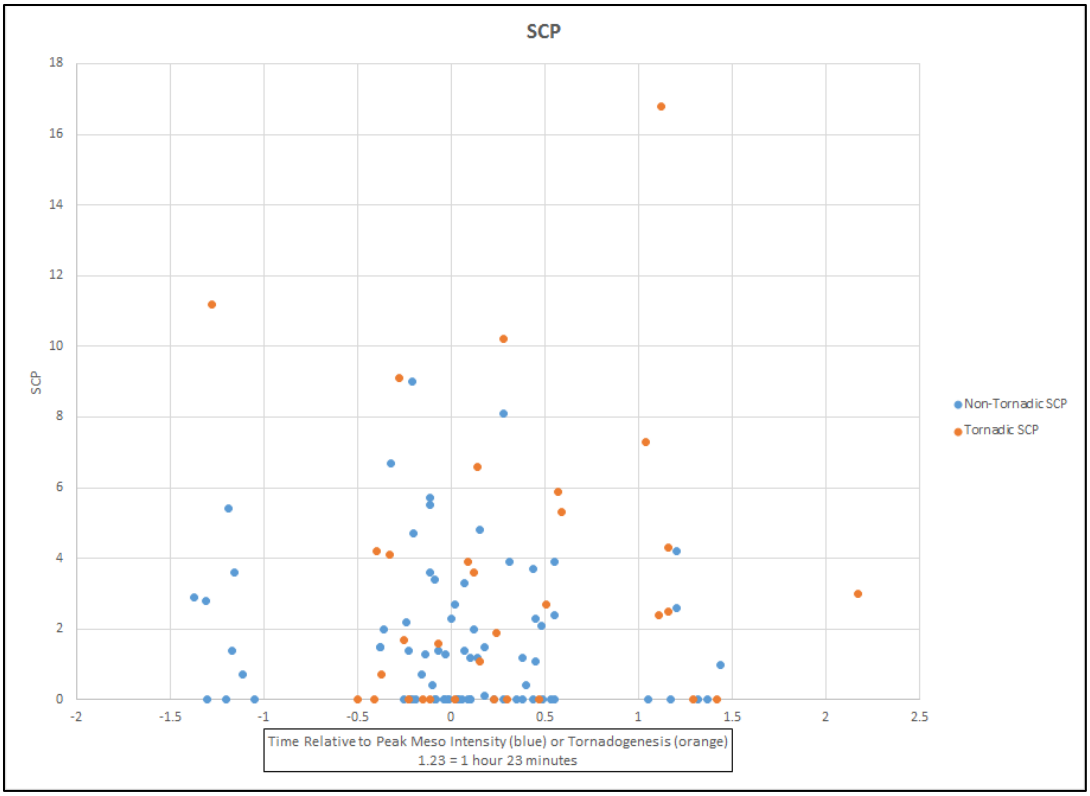

Figure 49. As in Fig. 13, but for SCP values.

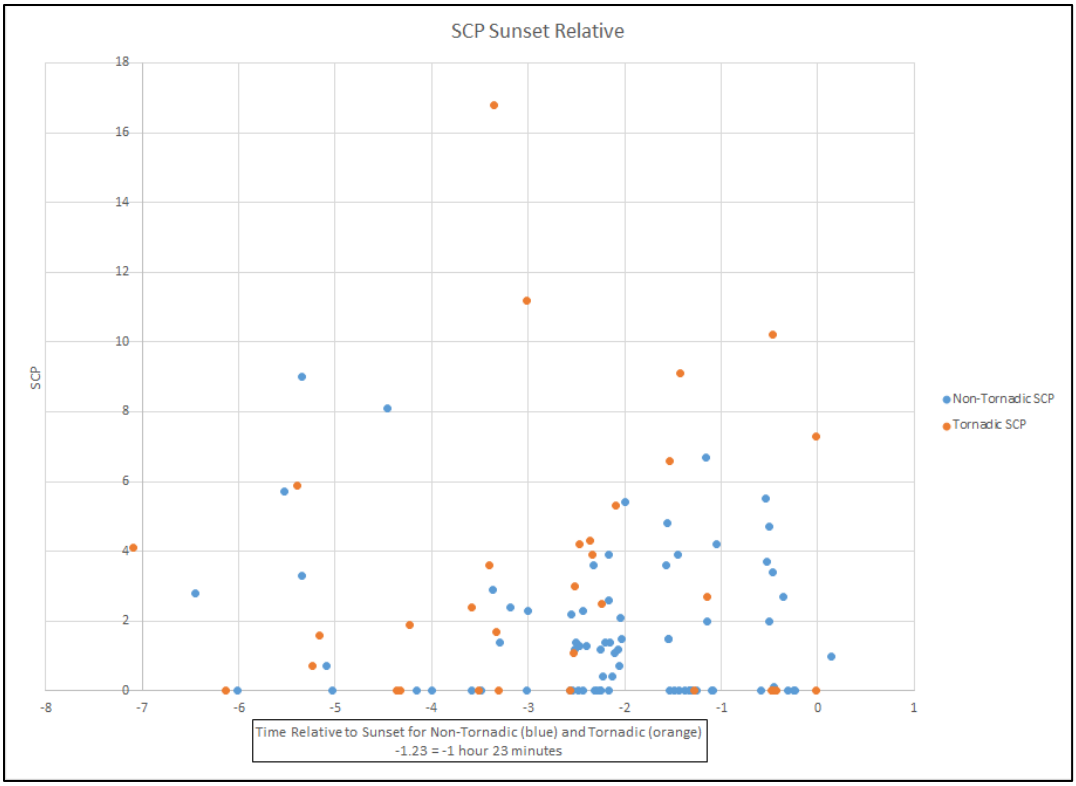

Figure 50. As in Fig. 14, but for SCP values.

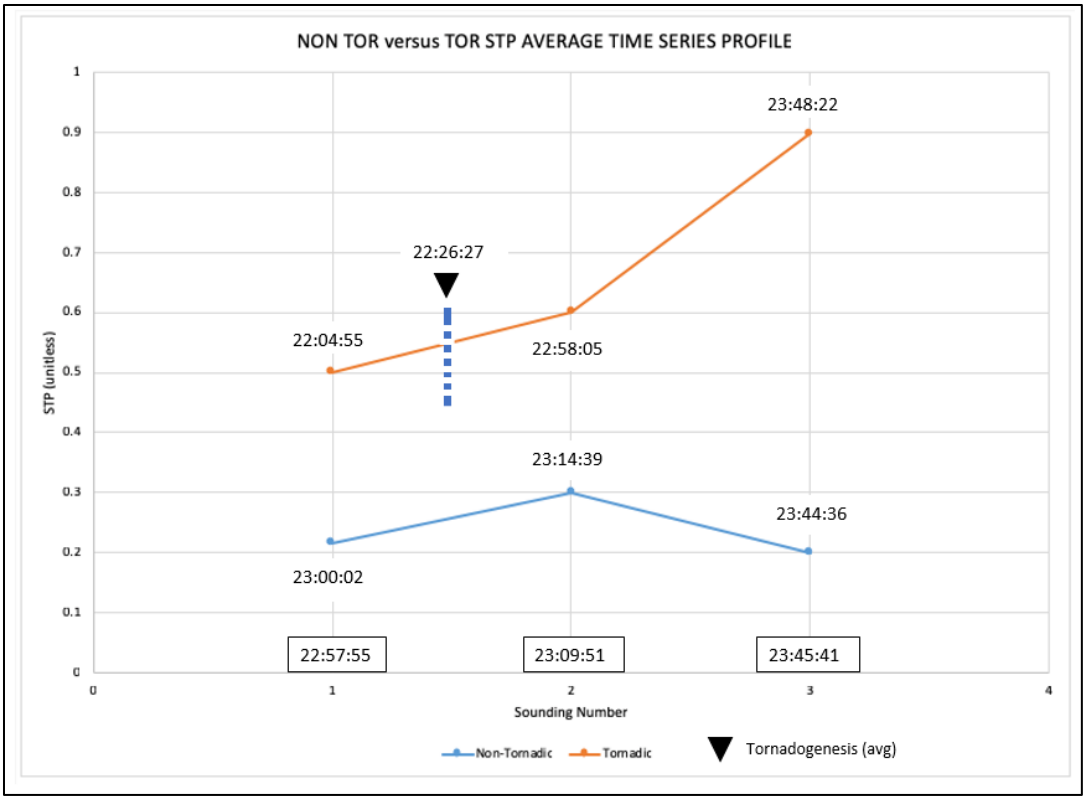

Figure 51. As in Fig. 11, but for STP (fixed) values.

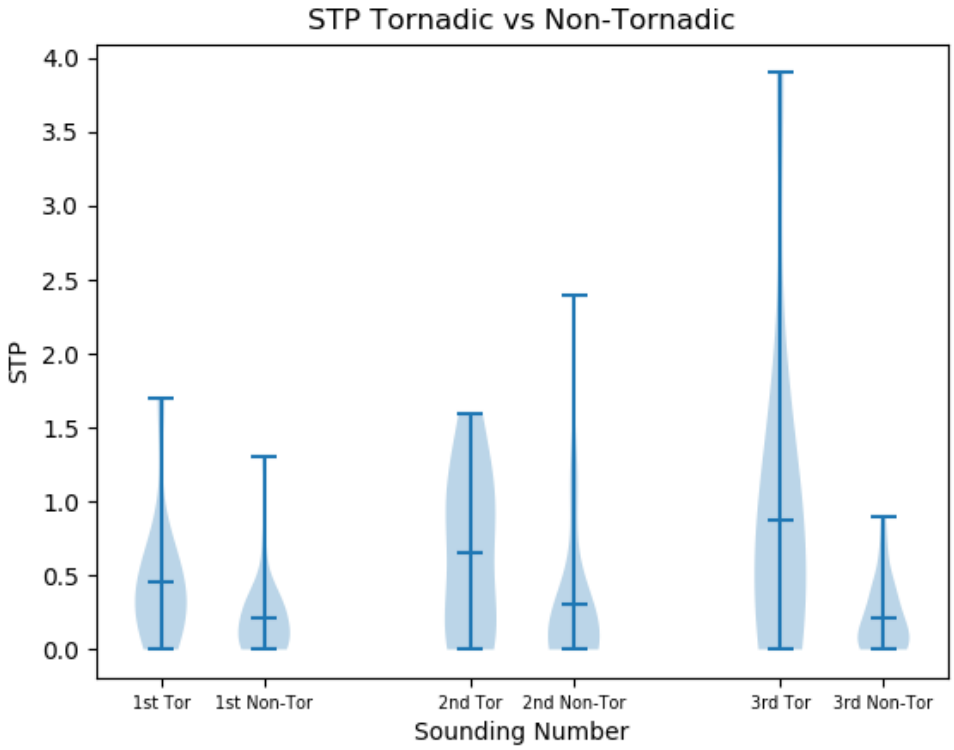

Figure 52. As in Fig. 12, but for STP (fixed) values.

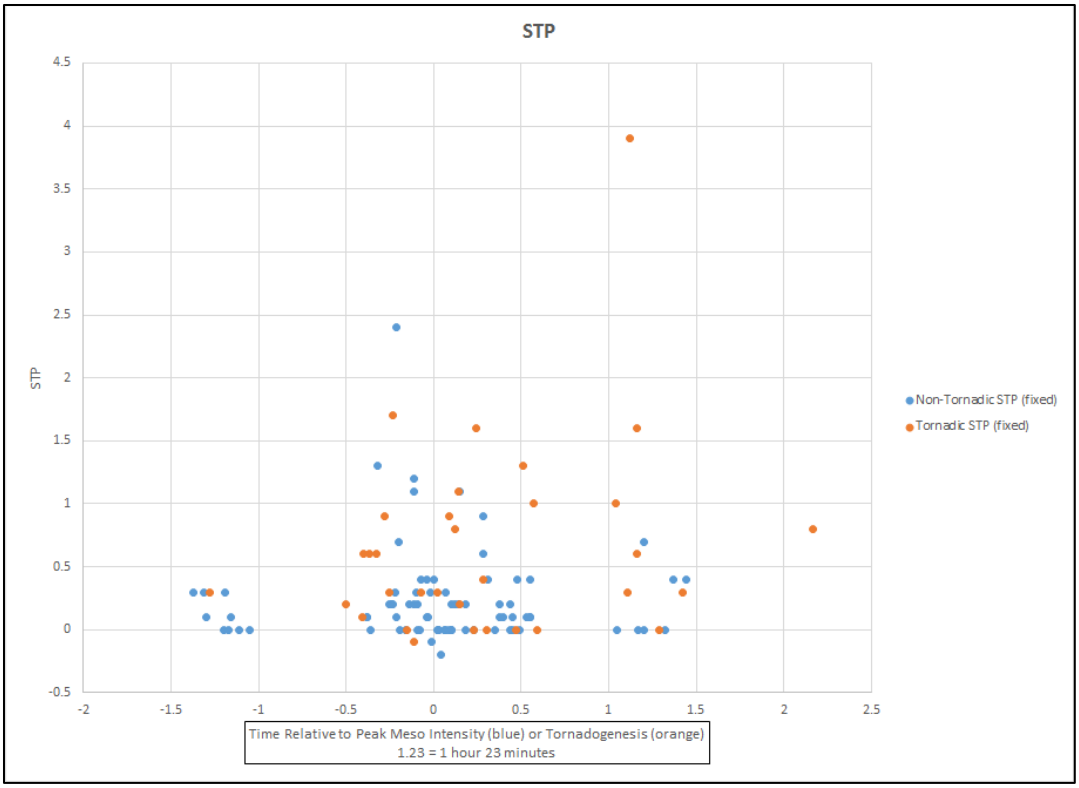

Figure 53. As in Fig. 13, but for STP (fixed) values.

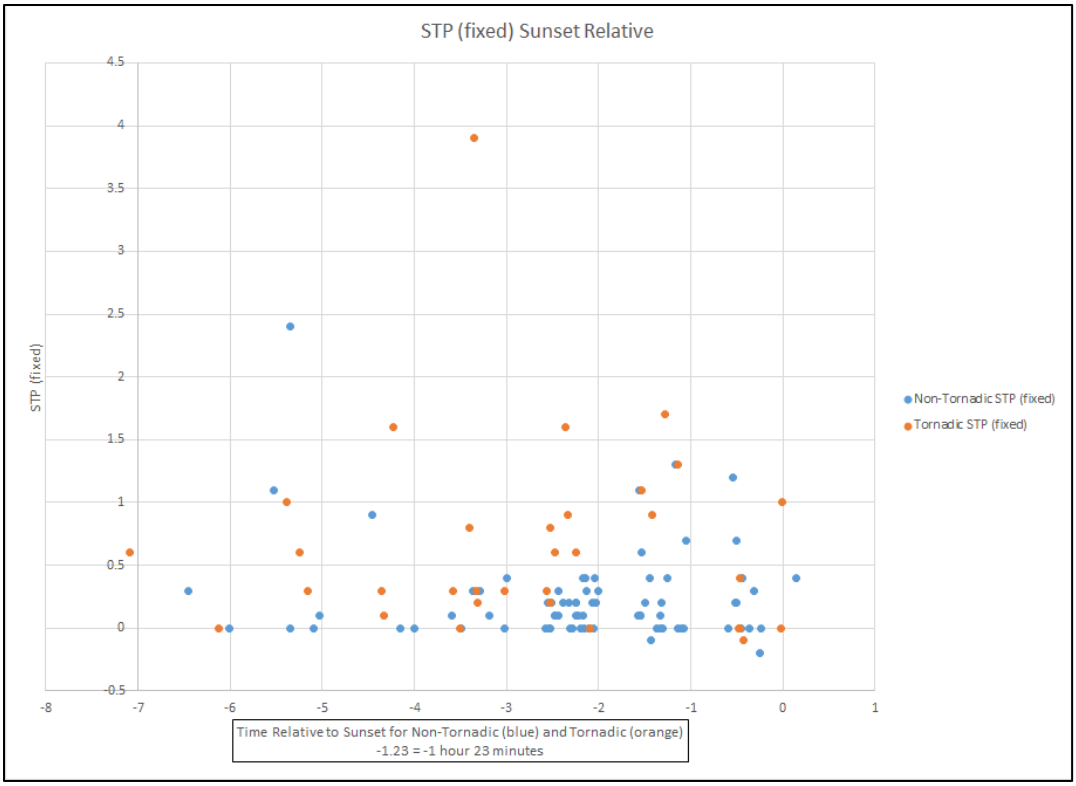

Figure 54. As in Fig. 14, but for STP (fixed) values.

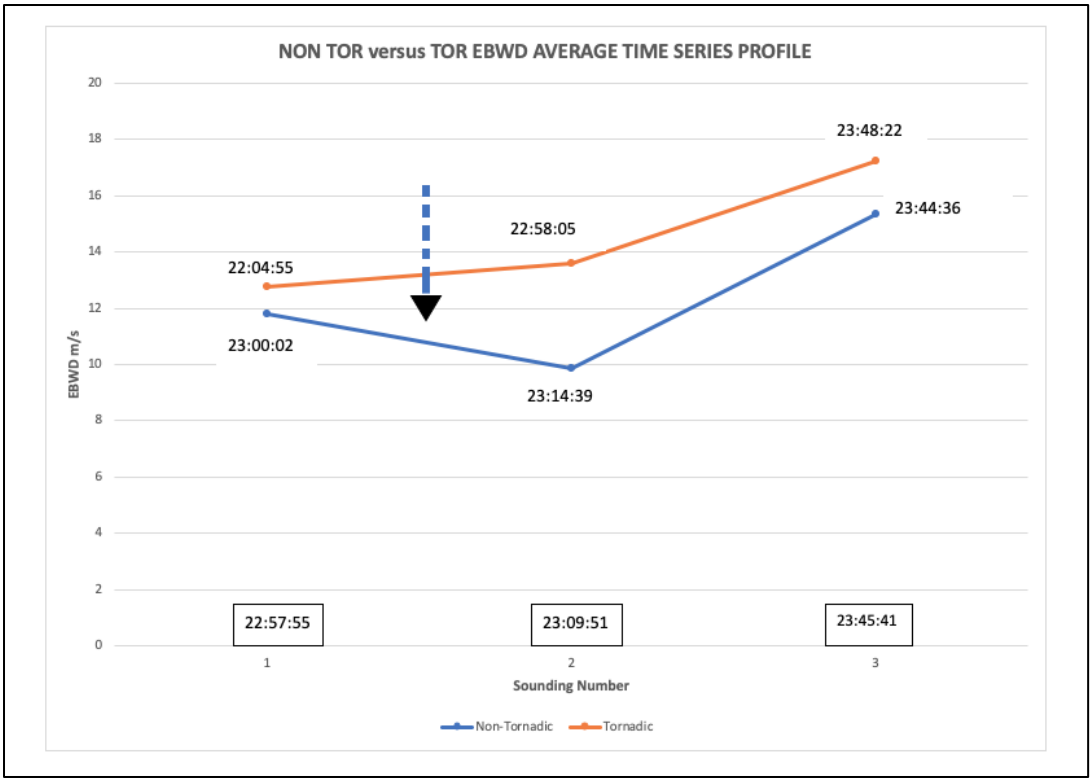

Figure 55. As in Fig. 11, but for EBWD values.

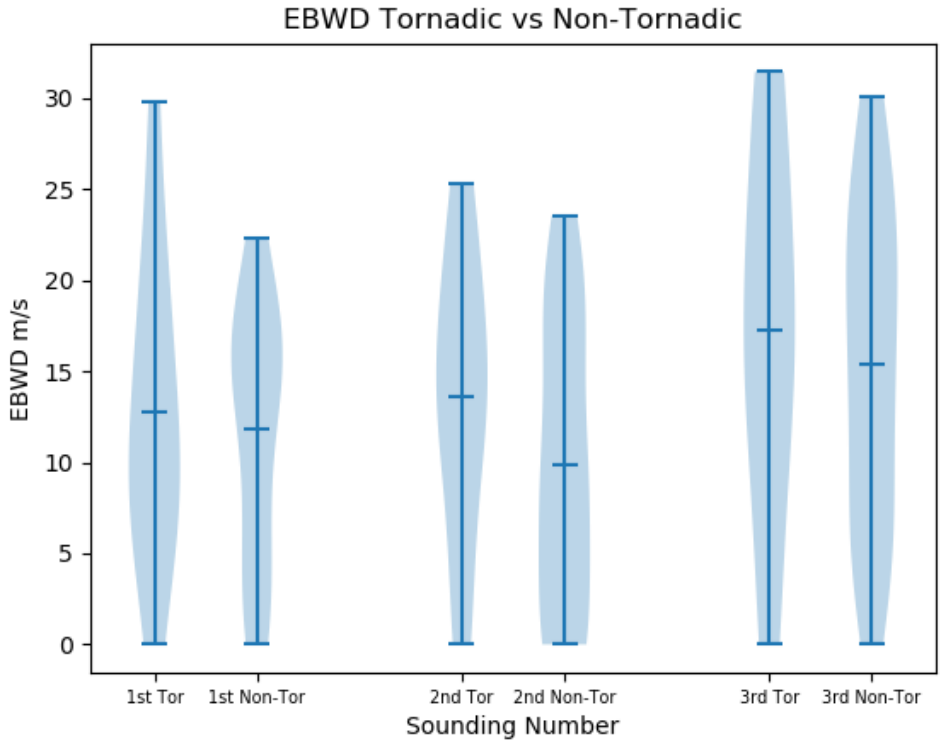

Figure 56. As in Fig. 12, but for EBWD values.

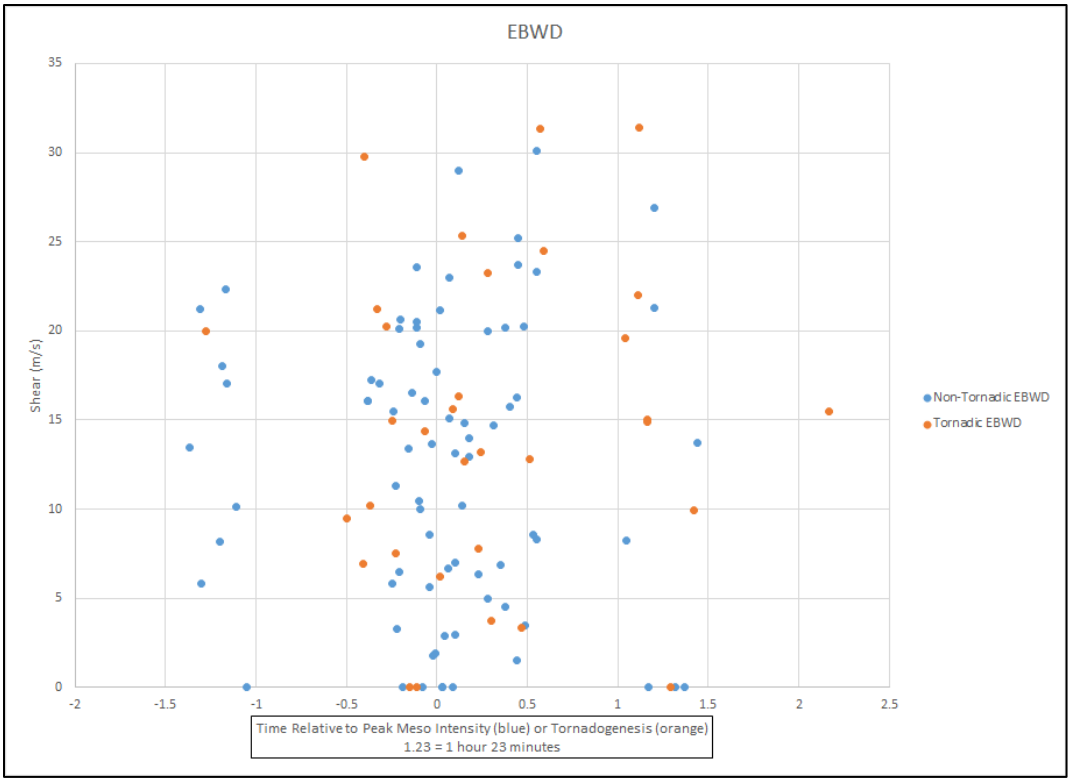

Figure 57. As in Fig. 13, but for EBWD values.

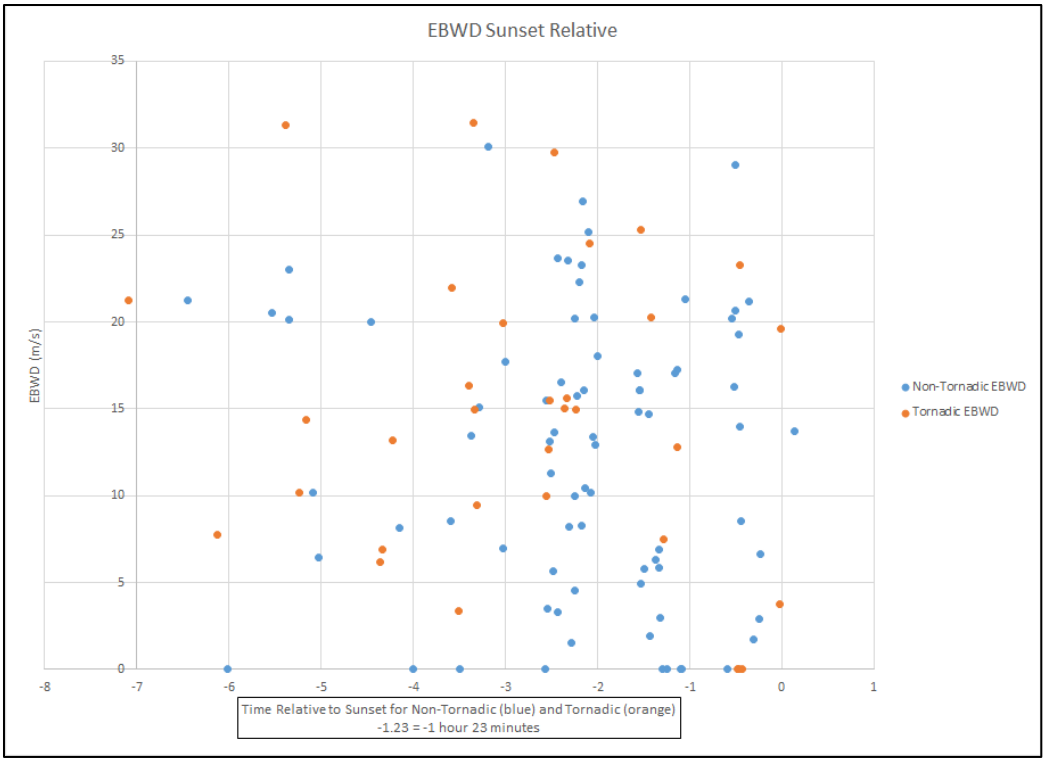

Figure 58. As in Fig. 14, but for EBWD values.

Table 4. Statistical Analysis- 2 means comparison (Non-Tornadic/Tornadic) displaying p-value of the entire 2-tailed dataset, t-difference, t value at 0.05/2-(0.025) for a 95% confidence interval and an explanation for if the tornadic or non-tornadic values are statistically different based on the results

Parameter	P-Value (Two-sided)	t-difference	t(0.025) for 95% CI	Statistical Difference at 5% Study Sample Size
SBCAPE	0.0922	-1.708	1.9951	No
SBCIN	0.535	0.623	1.9979	No
MUCAPE	0.0236	-2.308	1.9889	Yes
MUCIN	0.545	-0.609	1.9974	No
0-1 km SRH	0.0296	-2.258	2.0219	Yes
0-3 km SRH	0.6408	-0.47	2.0231	No
Effective SRH	0.0468	-2.044	2.10151	Yes
MULCL	0.0852	1.74	1.9859	No
MULFC	0.0796	1.773	1.9849	No
SCP	0.064	-1.914	2.0318	No
STP (fixed)	0.012	-5.45	2.0257	Yes
EBWD	0.1352	-1.514	2.0015	No

CHAPTER 5. DISCUSSION

The time series analysis and distributional violin plots provided some expected results with respect to values differing between the tornadic and non-tornadic cases as seen in previous literature. The goal was to understand any trends for the first three near inflow soundings and start visualizing any impacts that time of tornadogenesis, peak mesocyclone intensity and sunset may have on the parameter's trend. There were no significant trends not already know for distinguishing between tornadic and non-tornadic cases with the use of the violin plots. The distributions proved to be useful in confirming already understood information regarding the impact some parameters may have on tornado formation.

With temporal trends being the focus of this research, it is pivotal to review the results of parameter values relative to peak mesocyclone intensity, tornadogenesis, and sunset. There were not many parameters that experienced a trend relative to peak mesocyclone intensity or tornadogenesis but it is useful to mention the understood trends seen for how the tornadic values tended to be more favorable in these plots. MUCAPE, it is understood that the tornadic cases would generally experience higher values than the non-tornadic and that can certainly be seen here (Figs. 20-21). Buoyancy and instability are enhanced or decreased generally after tornadogenesis while being governed by mesoscale forcings like uplift, shear and moisture content as described in the background. When some of these values are enhanced (i.e, MUCAPE) they may contribute positively towards a stronger tilt and stretching to support tornadogenesis. This can be understood when reading Table 4 data on MUCAPE where the tornadic and non-tornadic values associated with the parameter were statistically significant. This can also be seen in

Figures 21 and 22 where the tornadic values were much larger than the non-tornadic with pretty constant variability with respect to time. CIN values did not have statistical difference at any levels being that any large variations in CIN values may very well "inhibit" the threat of these types of supercell thunderstorms.

A key ingredient for sustaining updraft rotation and low-level rotation is SRH; results from this study demonstrate that both 0 to 1 km SRH and effective SRH values were statistically significantly higher for tornadic cases, consistent with prior research (Table 4). Given the importance of SRH, it is unsurprising that STP was also significantly higher in tornadic than non-tornadic events. The only one of the four that experienced a distinguished amount of multicollinearity was STP (fixed) which is understood given the variables associated with the parameter in its equation that were also included in this analysis.

There was considerable parallel trends in both types of cases in regards to time of sunset relative data. This was a common theme for the majority of the parameters with overlap and no distinguishable differences between the tornadic and non-tornadic cases. Nonetheless, there were some parameters with trends leading up to sunset. MUCAPE and effective SRH both experienced values increasing on average when getting closer to time of sunset, both of which could be attributed to the development of the nocturnal low-level jet. SCP, with variables in its equation like the already stated statistically different parameters of MUCAPE and effective SRH, it can be understood why there would be some differences in the trends in this particular parameter. With all of these results in mind we can start to draw a conclusion based off the findings from this dataset with

respect to parameter interaction differences between tornadic and non-tornadic supercell environments on a temporal scale.

CHAPTER 6. SUMMARY AND FUTURE WORK

The goal in mind for this research was understanding any temporal trends related to discriminatory parameters in tornadic and non-tornadic near-storm environments observed. Spatially, this dataset has been researched thoroughly (Parker, 2014). With the purpose in mind, the dataset was observed in a few different ways using parameters that have been understood to be pivotal to both supercell formation and maintenance but also tornadogenesis. Overall time series was used for each parameter to encounter any progressive trends using the average times of the first three inflow near storm soundings observed in VORTEX2. The distribution of each parameter, both tornadic and non-tornadic was observed to witness any type of pattern within the temporal scale for both case types. Time relative data was then used to observe a more individualized trend with the data points with the observation of both peak mesocyclone intensity and tornadogenesis times along with time of sunset for each event. While performing these tasks, a statistical analysis was made to verify any potential findings that occurred with the dataset.

When it comes to finding any temporal trends at the time right before tornadogenesis, there did not appear to be any parameter that stood out as being a discriminatory variable with regards to this type of event. The time relative scatter plots displayed a considerable amount of variability with not a great deal of agreement in a trend. Some would have higher values depending on the case type which is well understood in these types of events with enhanced lifting, instability and moisture availability. One clear point is that there are however, parameters that are far more supportive for tornadic cases. There were larger values of 0 to 1 km SRH, Effective SRH,

MUCAPE and fixed STP in the tornadic cases which is verified in the statistical analysis (Table 4) in which all of these values were in the 0.05 threshold for the p-values needed for statistical difference at 5% study sample size. The general agreement in this research is while there are considerable differences in the parameter values between tornadic and non-tornadic supercell near-storm environments, there is not a single discriminatory parameter used for distinguishing between tornadic and non-tornadic environments. However, there are considerable overall differences in the environmental parameters values. Thus, though no discriminatory parameters were found there is still room for understanding more about other parameters along with soundings outside of the near-storm environment that could prove to be useful for understanding the temporal evolution of tornadic and non-tornadic near-storm environments in supercells.

REFERENCES

Bunkers, M. J. (2002). Vertical Wind Shear Associated with Left-Moving Supercells. Weather and Forecasting, 17(4), 845-855. doi:10.1175/1520-0434(2002)0172.0.co;2

-------, M. R. Hjelmfelt, and P. L. Smith, 2006a: An observational examination of long-lived Supercells. Part I: Characteristics, evolution, and demise. Weather and Forecasting, 21, 673–688, doi:10.1175/waf949.1.

Blumberg, W. G., Halbert, K. T., Supinie, T. A., Marsh, P. T., Thompson, R. L., & Hart, J. A. (2017). SHARPpy: An Open-Source Sounding Analysis Toolkit for the Atmospheric Sciences. Bulletin of the American Meteorological Society, 98(8), 1625-1636. doi:10.1175/bams-d-15-00309.1

Byers, H. R., & Braham, R. R. (1948). Thunderstorm Structure And Circulation. Journal of Meteorology, 5(3), 71-86. doi:10.1175/1520-0469(1948)0052.0.co;2

Coffer, B. E., & Parker, M. D. (2015). Impacts of Increasing Low-Level Shear on Supercells during the Early Evening Transition. *Monthly Weather Review, 143*(5), 1945-1969. doi:10.1175/mwr-d-14-00328.1

-------, and -------, (2017). Simulated Supercells in Non-tornadic and Tornadic VORTEX2 Environments. *Monthly Weather Review, 145*(1), 149-180. doi:10.1175/mwr-d-16-0226.1

Davenport, C. E., and M. D. Parker, 2015a: Observations of the 9 June 2009 dissipating Supercell from VORTEX2. Weather and Forecasting, 30, 368–388, doi:10.1175/waf-d-14- 00087.1.

-------, and -------, 2015b: Impact of environmental heterogeneity on the dynamics of a dissipating Supercell thunderstorm. Monthly Weather Review, 143, 4244–4277, doi:10.1175/mwr-d-15- 0072.1.

Davies-Jones, R., 1984: Streamwise Vorticity: The origin of Updraft rotation in Supercell storms. Journal of the Atmospheric Sciences, 41, 2991–3006, doi:10.1175/1520-0469(1984)041<2991:svtoou>2.0.co;2.

-------. (2015). A review of supercell and tornado dynamics. Atmospheric Research, 158-159, 274-291. doi:10.1016/j.atmosres.2014.04.007

Gropp, M. E., & Davenport, C. E. (2018). The Impact of the Nocturnal Transition on the Lifetime and Evolution of Supercell Thunderstorms in the Great Plains. Weather and Forecasting, 33(4), 1045-1061. doi:10.1175/waf-d-17-0150.1

Klees, A. M., Richardson, Y. P., Markowski, P. M., Weiss, C., Wurman, J. M., & Kosiba, K. K. (2016). Comparison of the Tornadic and Non-tornadic Supercells Intercepted by

VORTEX2 on 10 June 2010. *Monthly Weather Review, 144*(9), 3201-3231. doi:10.1175/mwr-d-15-0345.1

Klemp, J., 1987: Dynamics of Tornadic thunderstorms. Annual Review of Fluid Mechanics, 19, 369–402, doi:10.1146/annurev.fluid.19.1.369.

Lemon, L. R., and C. A. Doswell, 1979: Severe thunderstorm evolution and Mesocyclone structure as related to Tornadogenesis. Monthly Weather Review, 107, 1184–1197, doi:10.1175/1520-0493(1979)107<1184:steams>2.0.co;2.

Letkewicz, C. E., French, A. J., & Parker, M. D. (2013). Base-State Substitution: An Idealized Modeling Technique for Approximating Environmental Variability. *Monthly Weather Review, 141*(9), 3062-3086. doi:10.1175/mwr-d-12-00200.1

Markowski, P., Hannon, C., Frame, J., Lancaster, E., Pietrycha, A., Edwards, R., & Thompson, R. L. (2003). Characteristics of Vertical Wind Profiles near Supercells Obtained from the Rapid Update Cycle. *Weather and Forecasting, 18*(6), 1262-1272. doi:10.1175/1520-0434(2003)0182.0.co;2

---------, & Richardson, Y. P. (2009). Tornadogenesis: Our current understanding, forecasting considerations, and questions to guide future research. *Atmospheric Research, 93*(1-3), 3-10. doi:10.1016/j.atmosres.2008.09.015

---------, and ---------, 2010: Mesoscale meteorology in Midlatitudes. John Wiley & Sons, United States,.

Nowotarski, C. J., & Markowski, P. M. (2016). Modifications to the Near-Storm Environment Induced by Simulated Supercell Thunderstorms. *Monthly Weather Review, 144*(1), 273-293. doi:10.1175/mwr-d-15-0247.1

Parker, M. D. (2014). Composite VORTEX2 Supercell Environments from Near-Storm Soundings. *Monthly Weather Review, 142*(2), 508-529. doi:10.1175/mwr-d-13-00167.1

Rasmussen, E. N., & Blanchard, D. O. (1998). A Baseline Climatology of Sounding-Derived Supercell and Tornado Forecast Parameters. *Weather and Forecasting, 13*(4), 1148-1164. doi:10.1175/1520-0434(1998)0132.0.co;2

Rotunno, R. (1993). Supercell thunderstorm modeling and theory. *Geophysical Monograph Series The Tornado: Its Structure, Dynamics, Prediction, and Hazards,* 57-73. doi:10.1029/gm079p0057

--------- and J. Klemp, 1985: On the rotation and propagation of simulated Supercell thunderstorms. Journal of the Atmospheric Sciences, 42, 271–292, doi:10.1175/1520-0469(1985)042<0271:otrapo>2.0.co;2.

Thompson, R. L., R. Edwards, J. A. Hart, K. L. Elmore, and P. Markowski, 2003: Close proximity soundings within Supercell environments obtained from the rapid update cycle. Weather and Forecasting, 18, 1243–1261, doi:10.1175/1520-0434(2003)018<1243:cpswse>2.0.co;2.

---------, C. M. Mead, and R. Edwards, 2007: Effective storm-relative Helicity and bulk shear in Supercell thunderstorm environments. Weather and Forecasting, 22, 102–115, doi:10.1175/waf969.1.

Trapp, R. J., Tessendorf, S. A., Godfrey, E. S., & Brooks, H. E. (2005). Tornadoes from Squall Lines and Bow Echoes. Part I: Climatological Distribution. *Weather and Forecasting, 20*(1), 23-34. doi:10.1175/waf-835.1

Wurman, J., D. Dowell, Y. Richardson, P. Markowski, E. Rasmussen, D. Burgess, L. Wicker, and H. B. Bluestein, 2012: The Second verification of the origins of rotation in tornadoes experiment: VORTEX2. Bulletin of the American Meteorological Society, 93, 1147–1170, doi:10.1175/bams-d-11-00010.1.72

Ziegler, C. L., Mansell, E. R., Straka, J. M., Macgorman, D. R., & Burgess, D. W. (2010). The Impact of Spatial Variations of Low-Level Stability on the Life Cycle of a Simulated Supercell Storm. *Monthly Weather Review, 138*(5), 1738-1766. doi:10.1175/2009mwr3010.1